Ocean Modelling 84 (2014) 67–83

Contents lists available at ScienceDirect

Ocean Modelling

journal homepage: www.elsevier.com/locate/ocemod

Current–wave interaction in the Mississippi–Atchafalaya river plume on the Texas–Louisiana shelf

Zengrui Rong [a,b,*], Robert D. Hetland [a], Wenxia Zhang [a], Xiaoqian Zhang [a]

[a] Department of Oceanography, Texas A&M University, 3146 TAMU, College Station, TX 77843-3146, USA
[b] Physical Oceanography Laboratory, College of Physical and Environmental Oceanography, Ocean University of China, Qingdao 266100, PR China

ARTICLE INFO

Article history:
Received 2 April 2014
Received in revised form 24 September 2014
Accepted 27 September 2014
Available online 22 October 2014

Keywords:
Wave–current interaction
Mississippi river
River plume
Bottom roughness
Wave mixing
Vortex forces

ABSTRACT

Wave–current interaction over the Texas–Louisiana shelf, and its effects on the dispersal and mixing of the Mississippi–Atchafalaya river plume, have been investigated using the Coupled Ocean–Atmosphere–Wave–Sediment Transport (COAWST) Modeling System. The modeling system is driven by realistic wave and current conditions at the open boundaries and high frequency1-D wind measured from a nearby meteorological station. Skill analysis demonstrates that the model reproduces the wave and salinity fields reasonably well. Waves over the Texas–Louisiana shelf are dominated by locally forced wind seas, and generally propagate in the same direction as the winds. Investigation into the spatial differences in the effect of waves reveals two distinct dynamical regions: the Chenier shelf, the shelf region extending roughly offshore from Sabine Lake to Vermilion Bay, and the Louisiana Bight, the region between the Mississippi Delta and Terrebonne Bay. A variety of model runs are performed, where specific wave processes are either included or excluded, in order to isolate the processes acting in different regions. The Chenier shelf is mainly affected by wave enhanced bottom stress, whereas the Louisiana Bight is mostly affected by the surface wave induced mixing and 3-D wave forces. The wave enhanced bottom stress suppresses cross-shore exchange, and acts to trap more freshwater in the nearshore regions shallower than 50 m over the Chenier shelf. Wave enhanced bottom stress plays only a minor role in the Louisiana Bight, where the surface-trapped Mississippi plume rarely feels the bottom. The surface intensified wave mixing and 3-D wave forces reduce the surface salinity and weaken the stratification in the region associated with the thin recirculating Mississippi plume in the Louisiana Bight. Model results indicate that the surface wave mixing, the 3-D wave forces, and the wave bottom stress exhibit little interaction over the Texas–Louisiana shelf. Finally, we have demonstrated that the one-way coupling is capable of resolving the majority of wave effects over the entire shelf if the seasonal scale is of interest.

1. Introduction

Wave–current interaction is of prime importance in coastal water and nearshore regions (e.g. Lentz and Fewings, 2012; Prandle et al., 2000; Wolf and Prandle, 1999). Waves can be affected by the presence currents due to refraction, modification of bottom drag, and blocking (e.g., Vincent, 1979; Kudryavtsev et al., 1995; Ris et al., 1999). An impact of currents on waves modifies the wave frequency through Doppler shift, accompanied with a change in phase speed. Also, the water level has an influence on waves, by changing the depth felt by waves (e.g. Pleskachevsky and Kapitza, 2009). Conversely, the currents can be strongly forced and modified by waves. The effect of waves on mean flow are manifested through additional momentum and mass fluxes. Waves entering a shallow water region increase in amplitude and steepness, and finally break, resulting in onshore mass flux and changes of mean surface elevations called wave setup and setdown (Longuet-Higgins and Stewart, 1962). In the cross-shore direction, the vertical imbalance between the depth-uniform pressure gradient due to wave setup and the depth-varying momentum flux generates a near-bed seaward current, the undertow (Svendsen, 1984). While in the long-shore direction, the spatially non-uniform wave momentum flux provides a new forcing of a wave-driven long-shore current (Longuet-Higgins, 1970).

The importance of different wave processes on a given coastal environment has also been identified in many previous studies. For example, wave set-up during hurricanes could make significant contributions to the total storm surge and inundation area, a study

* Corresponding author at: Department of Oceanography, Texas A&M University, 3146 TAMU, College Station, TX 77843-3146, USA.
E-mail address: zengrui.r@gmail.com (Z. Rong).

http://dx.doi.org/10.1016/j.ocemod.2014.09.008
1463-5003/

in Massachusetts Bay showed that more area was flooded when wave effects were included (Beardsley et al., 2013). Wave–current interaction increase the bottom friction felt by currents and thus increase bottom stress. Xu et al. (2011) showed that the enhancement of bottom stress due to waves plays a key role in sediment suspension dynamics over the Texas–Louisiana shelf. By including the wave breaking mixing to a circulation model, Carniel et al. (2009) showed that the observed surface drifter tracks were more accurately reproduced than models that did not include wave breaking in the Adriatic Sea. Also, studies in the Yellow Sea demonstrated that models including mixing due to wave breaking improve the simulation of surface boundary layer thickness (Zhang et al., 2011).

Given the importance of wave's effects on oceanic currents and turbulence, great effort has been dedicated to the theory and robust numerical simulation of wave–current interactions (McWilliams et al., 2004; Ardhuin et al., 2008; Mellor, 2008; Warner et al., 2008; Uchiyama et al., 2010; Kumar et al., 2012; Bennis et al., 2011, and many others). In order to provide a complete view of wave–current interactions, the three dimensional primitive equation are modified to account for waves. The difficulty in 3-D wave–current models is properly describing the wave forces and vertically distributing them (Bennis et al., 2011). Pioneering work done during the past decade represents wave forces either in a gradient stress tensor (Mellor, 2003, 2008) or in vortex force formalism (McWilliams et al., 2004); both have been applied to the Regional Ocean Modeling System (ROMS, Warner et al., 2008; Kumar et al., 2012; Uchiyama et al., 2010) and other models (CH3D: Sheng and Liu, 2011; FVCOM: Wang and Shen, 2010). Since the development of 3-D coupled wave–current models is relatively new, we need to systematically investigate the numerical approach to wave coupling and the dynamical influences of waves in our specific model domain.

The Texas–Louisiana shelf is a broad continental shelf with strong buoyancy forcing from the Mississippi–Atchafalaya river system. The Mississippi river is the 7th largest river system in the world, exporting about 530 $km^3\ yr^{-1}$ freshwater into the shelf. This huge input of fresh water greatly enhances stratification over the shelf (DiMarco et al., 2010; Schiller et al., 2011; Zhang et al., 2012). The circulation over the Texas–Louisiana shelf can be viewed as a bottom-trapped buoyancy-driven flow modulated by seasonal winds (Zhang et al., 2014). During non-summer when winds are generally from the east, downwelling favorable, the buoyant plume water hugs the coastline and moves downcoast. In summertime, upwelling favorable winds push the plume upcoast, and the plume is trapped over the Louisiana shelf and further offshore, increasing stratification there. Numerous observation and modeling studies have been conducted in this region (e.g., Cho et al., 1998; Morey et al., 2003; Etter et al., 2004; Schiller et al., 2011; Hetland and DiMarco, 2008; Zhang et al., 2012). Some previous studies have included wave effects. Sheng et al. (2010) applied a coupled ocean-wave model to study the surge level and coastal inundation in the Northeastern Gulf of Mexico and emphasized the importance of wave effects in the 3-D model than the 2-D model. Xu et al. (2011) recognize the importance of wave enhanced bottom stress and focus on its effects on sediment transport. However, none of these studies deal directly with wave–current effects in relation to currents and tracer distributions over the shelf.

Waves have the potential to affect river plume dynamics. Recently, using an idealized model, Gerbi et al. (2013) studied the effects of surface wave mixing on river plume dynamics during upwelling favorable winds, with the wave breaking parameterized in the two equation turbulence sub-model (Craig and Banner, 1994). Both the plume structure and the response time were modified when breaking wave mixing was included (Gerbi et al., 2013). In addition to surface gravity wave breaking, waves might also alter the plume dynamics through enhanced bottom stress or wave vortex forces; these processes have not yet been addressed for the Mississippi–Atchafalaya river plume system.

This study takes advantage of the newly developed modeling system COAWST (Warner et al., 2008, 2010) to study the wave–current interaction over the Texas–Louisiana shelf. The goals of this study are to identify how waves and currents interact in the presence of a large river plume, and how waves alter the fresh water distribution and stratification within the plume on the shelf scale. The surf zone dynamics are not included, since this specific study focus more on shelf processes and interactions between the inner- and mid-shelf. In this paper, we demonstrate that the fully resolved wave dynamics in the coupled model significantly modifies the plume structure and thus the stratification, not only during extreme weather conditions but also in fair weather conditions. Also, we find that different wave effects are dominant in different regions of the plume. Finally, we find that if seasonal scale is of interest, it is not necessary to include two-way coupling for our large domain, it is sufficient to specify the wave field through an independent simulation, and then apply those wave effects to the hydrodynamic model.

2. Methodology

The COAWST modeling system (Warner et al., 2008, 2010) is used in this study. The system couples the three-dimensional ROMS hydrodynamic model with the SWAN wind-wave generation and propagation model. Coupling with the Weather Research and Forecasting (WRF) model is deactivated in order to simplify the analysis and focus on wave–current interactions.

2.1. ROMS ocean model

The oceanic circulation model used in COAWST is the Regional Ocean Modeling System (ROMS) (Haidvogel et al., 2000; Shchepetkin and McWilliams, 2005). ROMS is a hydrostatic, primitive equation ocean model that solves the Reynolds averaged form of the Navier Stokes equations. We use a model domain that covers much of the Mississippi and Atchafalaya river plume region, initially developed by Hetland and DiMarco (2008). An orthogonal curvilinear coordinate system is designed to follow the coastline (Fig. 1). High resolution is placed in the inner shelf region to resolve the river plume, with the highest between the Mississippi Delta and the mouth of Atchafalaya Bay. The grid spacing is less than 1 km in the cross-shelf direction and 2–3 km in the along-shelf direction over the inner shelf region but increases to as coarse as 20 km offshore near the open boundaries. The total number of grid points is 128×63. The model has 30 layers in the vertical with the minimum depth setting to 3 m. We use the Generic Length Scale (GLS, k–ε) turbulence closure scheme to calculate the vertical eddy viscosity and diffusivity (Umlauf and Burchard, 2003; Warner et al., 2005). In the absence of waves, a quadratic stress is exerted at the bed, assuming that a logarithmic velocity profile in the bottom boundary layer. The drag coefficient is determined by $C_d = \max(C_z, 0.0025)$ where $C_z = \kappa^2 / \ln\left(\frac{\Delta z}{z_0}\right)^2$, $\kappa = 0.4$ is von Karman's constant, and the bottom roughness parameter z_0 is chosen to be 1 mm (Hetland and DiMarco, 2012; Marta-Almeida et al., 2013).

The open ocean boundary condition for the barotropic component consists of a Chapman/Flather boundary condition for depth averaged flow and sea surface elevation (Chapman, 1985; Flather, 1976). The open boundary condition for the baroclinic component is Orlanski-type radiation condition (Orlanski, 1976). A nudging region is specified along the six outer cells of the model domain, where the ROMS model is nudged toward HYCOM daily data. The nudging time scale used is eight hours at the boundaries with a

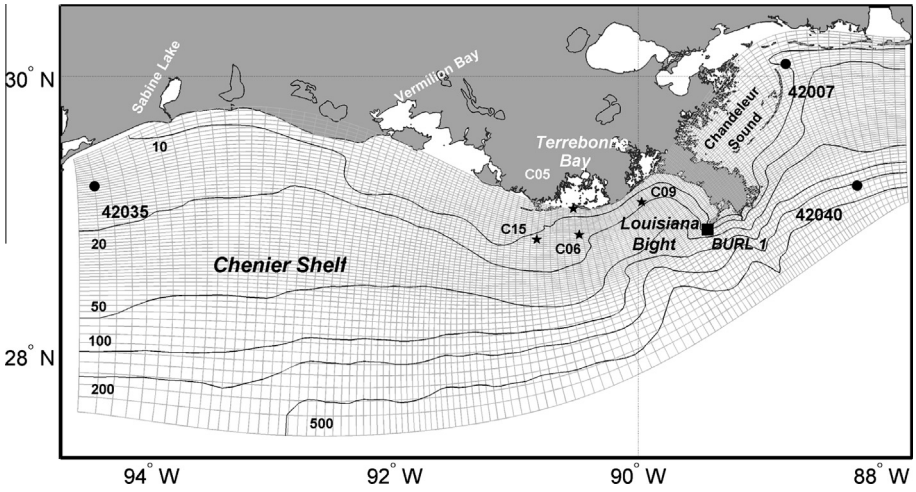

Fig. 1. ROMS model domain and the bathymetry map. The NDBC buoys are marked as solid circles and the WAVCIS buoys are marked as stars. The BURL 1 C-MAN meteorological station is marked as a solid square.

sinusoidal decay to the interior. The same nudging time scale is used for the incoming and outgoing information. The advantage of this nesting approach has been discussed in Barth et al. (2008) and Marta-Almeida et al. (2013). Freshwater inputs from the Mississippi and Atchafalaya rivers are specified using daily measurements of the U. S. Army Corps of Engineers. At surface, the short wave radiation, air temperature, humidity and atmosphere pressure are specified using climatological measurements (da Silva et al., 1994). Wind forcing is provided with 10 min periodicity from the weather station BURL 1 C-MAN (89.428 W × 28.905 N), close to the mouth of the Southwest Pass. The Coupled Ocean Atmosphere Response Experiment (COARE) 3.0 bulk flux algorithms are used to estimate the wind stress and the heat flux in ROMS. In COARE, the default Charnock-type relationship (Charnock, 1955) is used to parameterize the surface roughness in bulk fluxes. The horizontally uniform wind is a reasonable approximation, due to the large, O (400 km), horizontal spatial scales of the wind field in the study region (see Wang et al., 1998). Usage of real wind with very high temporal resolution is an advantage since the inclusion of wind peaks and the sea breeze is essential to wind mixing and wave generation. There are several previous modeling studies using the same single point wind and these studies show that the idea of single point wind forcing works out fine in terms of model skills (Hetland and DiMarco, 2012; Marta-Almeida et al., 2013; Zhang et al., submitted for publication). Further details of the model configuration can be found in Marta-Almeida et al. (2013).

2.2. SWAN spectral wave model

The wave model is Simulating Waves Nearshore (SWAN). SWAN is the third generation shallow water spectral wave model that includes wave propagation, refraction due to currents and depth, generation by wind, dissipation (white-capping, bottom friction, depth induced breaking), and nonlinear wave–wave interactions (Booij et al., 1999). In the coupled system, the free surface elevations and currents are provided to SWAN by ROMS. There are two ways that currents affect waves: first, the effective wind of generating waves is modified by the ocean current, and the effective fetch also changes in the presence of current (for example as in Kara et al., 2007); second, the current modifies the wave action balance equation through changes in propagation velocity of wave energy (see for example, Fan et al., 2009; Benetazzo et al., 2013). The currents were computed according to the formulation presented by Kirby and Chen (1989), in which the vertical distribution of the current profile is taken into account, as well as the relative water depth of the surface waves.

In the present application, the SWAN model is run and coupled to the same grid as the ROMS model. Twenty-five frequencies (0.01–1 Hz) and thirty-six directional bands are used. The SWAN model boundary is provided by the output of the 10 arc minute Northern Atlantic regional wave spectral model WAVEWATCH III, which is nested to a global wave model (ftp://polar.ncep.noaa.gov/pub/history/waves/). The data output is every 3 h. Local wave generation is specified by applying wind from the BURL 1 C-MAN station uniformly over the grid, consistent with ROMS. Wave growth by wind is computed with the exponential term of Komen et al. (1984) with default coefficients. The SWAN model then provides wave properties – such as significant wave height, mean wave direction, surface peak wave period, mean wave length, wave energy dissipation, percent of breaking waves, etc. – as input to ROMS for the estimation of bottom shear stress, vortex forces, and wave mixing.

2.3. COAWST system setup

The effects of surface waves on the circulation model are coupled mainly through three physical mechanisms:

(i) *Wave enhanced bottom shear stress.* The presence of waves increase the effective bottom roughness felt by the mean flow (e.g. Grant and Madsen, 1978). The bottom boundary layer determines the stress exerted on the flow by the bottom, which is used in the Reynolds-averaged Navier–Stokes equations as boundary conditions for momentum. COAWST has implemented a number of choices for wave–current bottom boundary layer models (Warner et al., 2008) and has coupled them with calculations of bottom roughness. In the present study, the wave–current bottom boundary layer model of Madsen (1994) named as SSW_BBL in COAWST is used (Warner et al., 2008).

(ii) *Wave enhanced mixing.* Wave breaking leads to mixing of momentum in the upper water column (Kitaigorodskii et al., 1983; Terray et al., 1996). This effect is considered as a surface flux of turbulent kinetic energy (Carniel et al., 2009; Kumar et al., 2012). In the absence of wave breaking, the surface boundary condition for turbulent kinetic energy is no flux through the boundary, and the boundary condition for the turbulent length scale is set to the surface roughness length. When wave breaking is included, however, changes

are made to the turbulent kinetic energy through the sea surface and the surface roughness length (Carniel et al., 2009; Kumar et al., 2012). Kumar et al. (2012) suggest usage of Carniel et al. (2009) kind of deep water wave breaking for deep water applications and the formalism of Feddersen and Trowbridge (2005) in the surf zone. In the present study, the Carniel et al. (2009) option, CRAIG_BANNER in COAWST, is used, together with a Charnock-type relationship to define the surface roughness length (Charnock, 1955).

(iii) Excessive momentum flux within the circulation due to the presence of waves. Additional wave forces can be exerted as either a gradient stress tensor or as a vortex force depending on the decomposition method used in the nonlinear advection terms. In the present application, we use the vortex force method which was proposed by McWilliams et al. (2004) and then implemented to ROMS-UCLA by Uchiyama et al. (2010) and COAWST by Kumar et al. (2012). The vortex force formalism introduces several additional forces in the Reynolds-averaged Navier–Stokes equations: the Bernoulli head, the Stokes–Coriolis forces, the vortex forces and the non-conservative wave forcing. The non-conservative wave forcing is further decomposed into the surface and bottom streaming terms, and wave breaking terms (Kumar et al., 2012).

The coupled modeling system is applied to assess the impact of waves on simulation of stratification and to identify the dominant processes acting in wave–current interactions. To achieve this, a series of different cases were run, including two-way fully coupling, one-way coupling, and process-oriented cases. The process-oriented cases examine particular wave processes in isolation by neglecting the other forces within the modeling framework. Table 1 summarizes the configurations for all the model runs. The model was initialized on January 1, 2004, with the addition of waves on February 1, 2005 when WAVEWATCH III wave data were available and ran to December, 31, 2009. Different time steps were used for ROMS and SWAN. In ROMS a 20 s baroclinic time step was used with a model-splitting ratio of 30. SWAN was run in non-stationary mode with a time step of 300 s. The coupling between ROMS and SWAN was done synchronously with 10 min time interval. The long term run has the advantage to reveal the common quality and the essential features, with the multiple years acting as an ensemble. Without a long term average, our simulations would be dominated by the small-scale chaotic features reported by Marta-Almeida et al. (2013).

3. Model assessment

3.1. Wave assessment

Wave heights from the One-Way-Couple wave model are compared with three NDBC buoys (Fig. 1). Effects of the circulation model on waves are not considered in this run (Table 1). The NDBC buoys are located close to the open boundary, so that model results at the NDBC buoy sites are affected by both the WAVEWATCH III boundary condition and the internal SWAN model. Year 2008 is selected for comparison because the most wave data are available for this year. As shown in Fig. 2, the model simulation follows the observations closely; the model skill is higher than 0.94 at buoys 42,007 and 42,040. The relatively lower model skill at buoy 42,035 could either be due to the limitation of WAVEWATCH III in resolving shallow water waves or due to the bulk wave boundary used by SWAN. The fairly good consistency between the simulation and observations indicates that our open boundary is doing well and the WAVEWATCH III results are able to provide reasonable wave estimates at the boundaries.

In addition to the NDBC buoys, model simulated significant wave heights are also compared to four WAVCIS buoys (http://wavcis.csi.lsu.edu/), managed by the Louisiana State University (Fig. 3). The WAVCIS buoys are located relatively far from the boundary, in the nearshore region (Fig. 1). The simulated wave field is in fairly good agreement with the observations. The averaged RMS error, correlation coefficient and skill are 16 cm, 0.88 and 0.91, respectively (see Zhong and Li, 2006 for definitions). We conclude that the wave model is capable of resolving the basic wave characteristics over the Texas–Louisiana shelf.

Given the reasonable ability of the model to predict the wave field, we now investigate the relationship between winds and waves over the shelf. Fig. 4 shows the wind and wave rose in four selected months of 2008, February, May, August and November, representing winter, spring, summer and fall, respectively. The wind vectors are observations at the weather station BURL 1 C-MAN, the same as the model forcing, while the wave vectors are model predictions. The colored sectors in Fig. 4 indicate wave direction or direction the wind vector is directed towards, colors show the wind speed and the peak wave period, respectively. As shown in Fig. 4, waves propagate generally northeastward in February and May, the same direction as the wind vectors. In August, the wind switches to upwelling favorable and the wave propagation turns to match the wind (Fig. 4e and f). In the transition season of fall, both the wind and the wave are relatively dispersed but again show similar patterns (Fig. 4g and h). The consistency between wind and waves reveals the importance of local wind in generating waves over the Texas–Louisiana shelf. The wave field is dominated by locally generated wind seas with periods generally less than 8 s, but could reach as much as 14 s, indicating swell from the outer shelf might be occasionally important.

Wave characteristics will be altered when propagating in an ambient current. Wave period will become longer (shorter) when propagating following (opposing) the direction of the current. The corresponding wave frequency and wave length will change accordingly. Changes in water depth also lead to changes in wave propagation, producing shoaling, refraction or wave breaking, which in turn, leading to changes in wave characteristics. Typically regions with strong currents identify regions of significant wave–current interaction. The effects of the circulation model on the wave field are examined by a selected location of C-09 (Fig. 1), in the recirculating bulge region, with particularly strong current. Including currents from the circulation model does have some influence on the wave field, especially for the wave direction and wave length (Fig. 5), but generally less than 10° and 3 m, respectively. Changes to the significant wave height are relatively small. Even during hurricane Ike, significant wave height changes by

Table 1
Model configurations for all numerical experiments.

	Ctrl ROMS	Two-Way-Couple ROMS ⟺ SWAN	One-Way-Couple ROMS<=SWAN	Couple-TKE ROMS ⟺ SWAN	Couple-BBL ROMS ⟺ SWAN	Couple-VF ROMS ⟺ SWN
Surface TKE	N/A	On	On	On	Off	Off
3-D wave force	N/A	On	On	Off	Off	On
Wave BBL	N/A	On	On	Off	On	Off
	No couple	Two-Way Fully Couple	One-Way Couple	Two-Way Partly Couple		

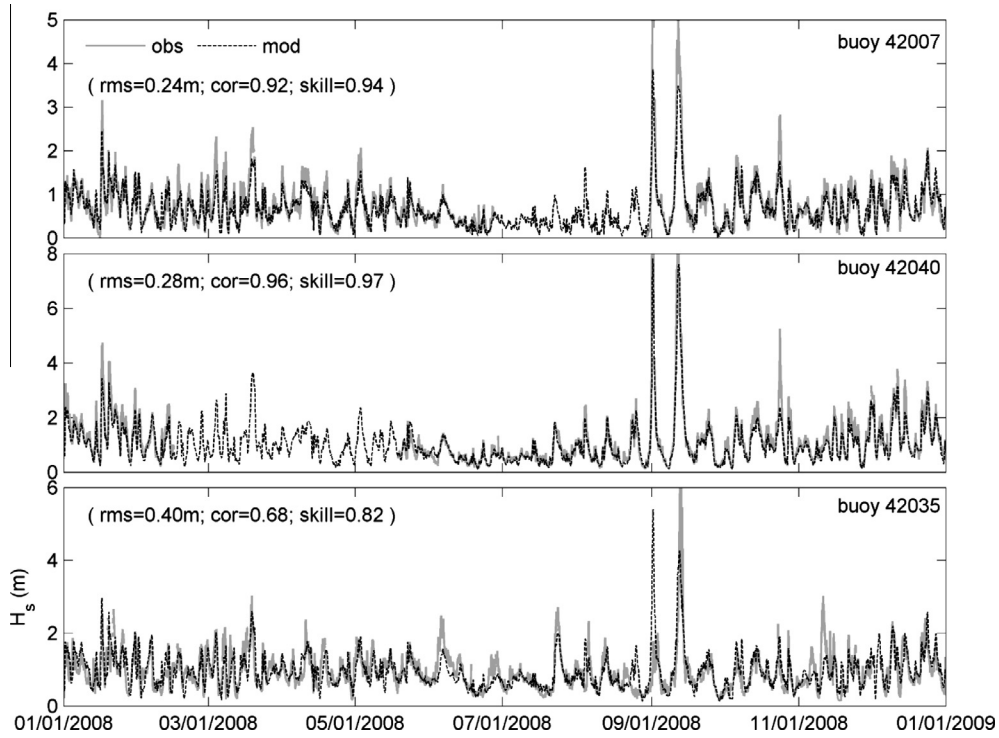

Fig. 2. Comparison of time series between model-simulated (black dashed) and observed (gray solid) significant wave height at three NDBC buoys (their locations given in Fig. 1). Note that the range of the *y*-axis is different for the three sub-panels.

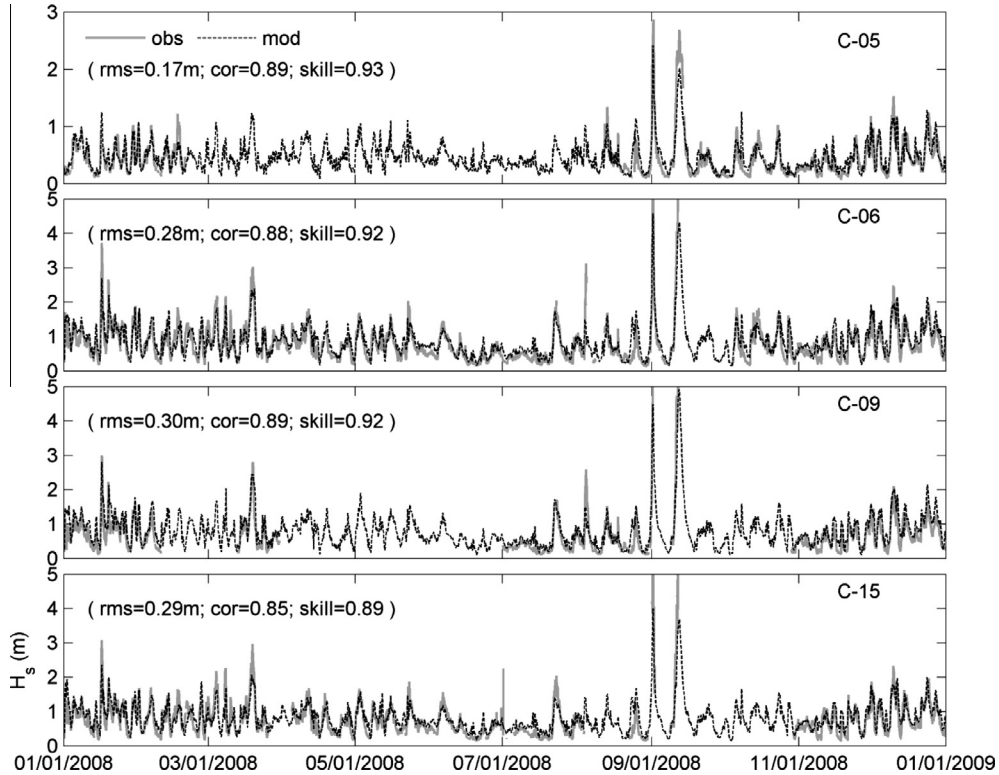

Fig. 3. Comparison of time series between model-simulated (black dashed) and observed (gray solid) significant wave height at four WAVCIS buoys (their locations given in Fig. 1). Note that the range of the *y*-axis is different for the four sub-panels.

about 0.4 m compared to the highest value of about 6 m. The RMS and relative difference of significant height (8 cm, 9%), surface peak wave period (0.7 s, 11%), mean wave direction (10°, 8%) and mean wave length (3 m, 11%) reveal that the influence of currents is generally small (Fig. 5). The spatial distribution of the relative differences shows that the largest differences occurs near the

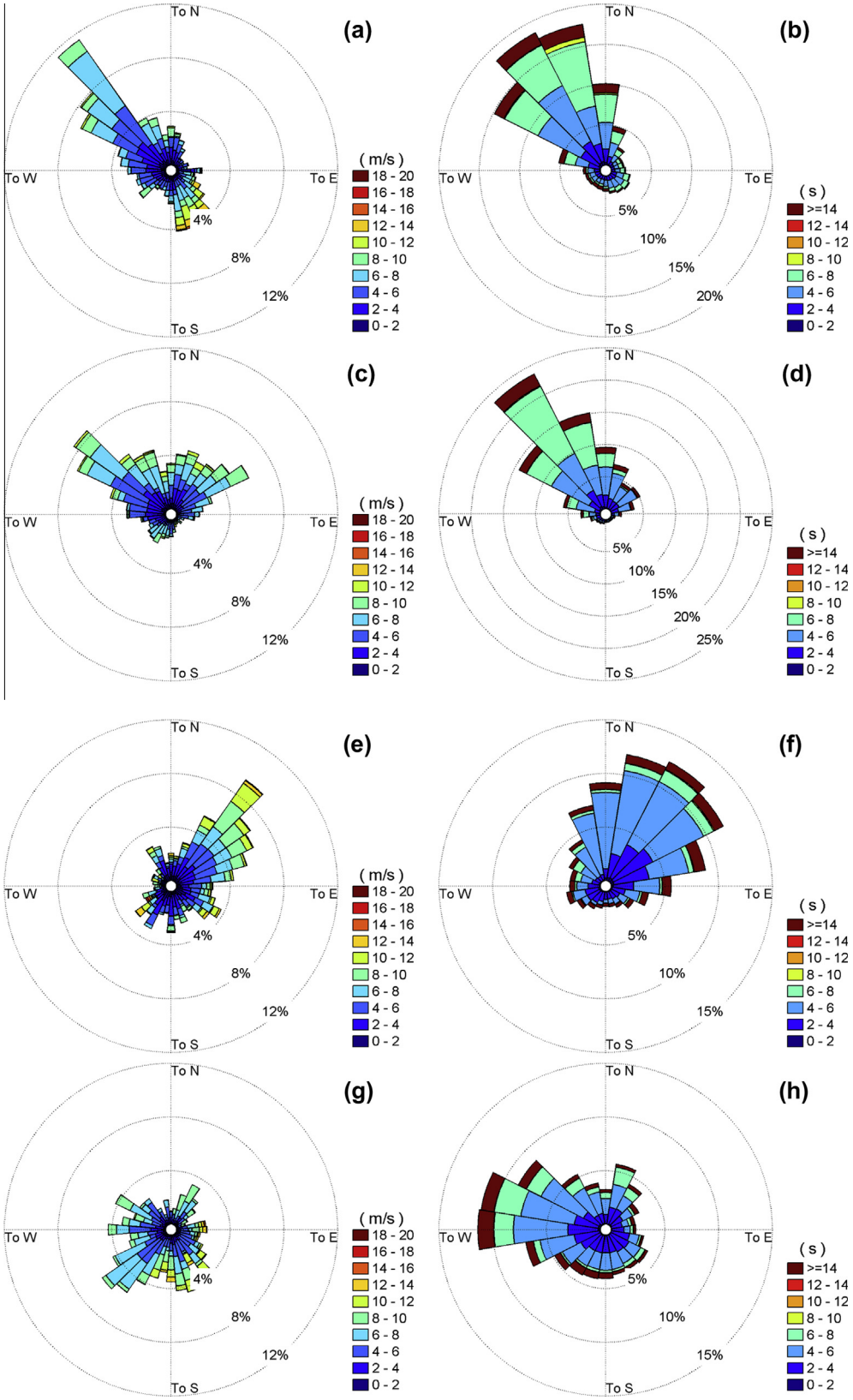

Fig. 4. Direction frequency of wind (left column) and waves (right column) at (a, b) February, (c, d) May, (e, f) August and (g, h) November. Sectors indicate the wave direction or the direction the wind vector is directed towards. Colors are the wind speed and the peak wave period, respectively. The wind vectors are observed at the weather station BURL 1 C-MAN, the same as the model forcing, while the waves are model predictions.

Mississippi Delta and in shallow regions with water depth less than 30 m, with the differences between the coupled and uncoupled run being generally less than 10 percent (not shown here). The current over the Texas–Louisiana shelf is typically less than

50 cm/s, and so currents are weaker than other regions with strong wave–current interaction (Ardhuin et al., 2012), so that our finding that circulation has a relatively weak effect on the wave field is reasonable.

3.2. Ocean model assessment

The present ocean model was initially developed by Hetland and DiMarco (2008) to investigate the mechanisms controlling hypoxia over the Texas–Louisiana shelf. It was originally forced by climatological WOA boundaries. Comparison with hydrographic and moored observations of temperature, salinity, and current velocity confirmed that it was able to reproduce the broad-scale plume structure and seasonal patterns (Hetland and DiMarco, 2012). The same model and configuration then acted as the ocean module to study the phytoplankton variability (Fennel et al., 2011) and sediment transport processes (Xu et al., 2011) over the Texas–Louisiana shelf and produced plausible results when comparing with observations. Using the same base model, Marta-Almeida et al. (2013) showed that nesting this shelf-scale model to a parent circulation model, e.g. HYCOM, improved the salinity skill compared to the same model using climatological boundary conditions. A recent study by Zhang et al. (submitted for publication) further showed that the nested model reproduced the stratification reasonably well. We use the same model configuration as Marta-Almeida et al. (2013) except that the turbulence closure scheme has been switched from Mellor–Yamada 2.5 to Generic Length Scale (GLS, k–ε) turbulence closure scheme. As will be shown below, this improves the salinity skill slightly.

Here we mainly assess the model capability in simulating a realistic salinity field. We use salinity profiles collected from the Mechanisms Controlling Hypoxia (MCH) project to assess the model skill. MCH collected vertical profiles of salinity, temperature and dissolved oxygen concentration data from March to August for Year 2004 though 2009 except 2006 (see Marta-Almeida et al., 2013 for details). A total of 840 profiles from 11 cruises over 2005–2009 were employed in this study. The model skill is defined as

$$skill = 1 - \frac{\sum_{i=1}^{N}(o_i - m_i)^2}{\sum_{i=1}^{N}(o_i - c_i)^2} \quad (1)$$

where o_i are the observations, m_i the model results at the same location and times, c_i is the climatological data, and N is the total number of observations (Hetland, 2006). This model skill evaluates model performance based on climatology. If the variance of model error is smaller than the variance of observations, then the model skill is positive. A higher model skill indicates that the model can reproduce the observations more closely, while a lower model skill suggests the model might be more dynamically active. Fig. 6 shows the model skill in predicting salinity based on all MCH salinity profiles. For this skill assessment, data through the whole water column are used, and the error presented for each profile is the vertically averaged value normalized by the standard deviation of the observed salinity relative to the climatological salinity. The overall model skill is 0.62, indicating that the model reproduces about 60% more variance beyond that already described by the seasonal climatology. The errors are generally randomly distributed in space, with predicted salinity higher at some stations and lower at others, indicating the active sub-mesoscale eddies on the shelf (Hetland and DiMarco, 2012). A comparison with the former run shows that switching the turbulence closure scheme from Mellor–Yamada 2.5 to k–ε (GLS) increases the salinity skill by about 0.09 for this specific comparison.

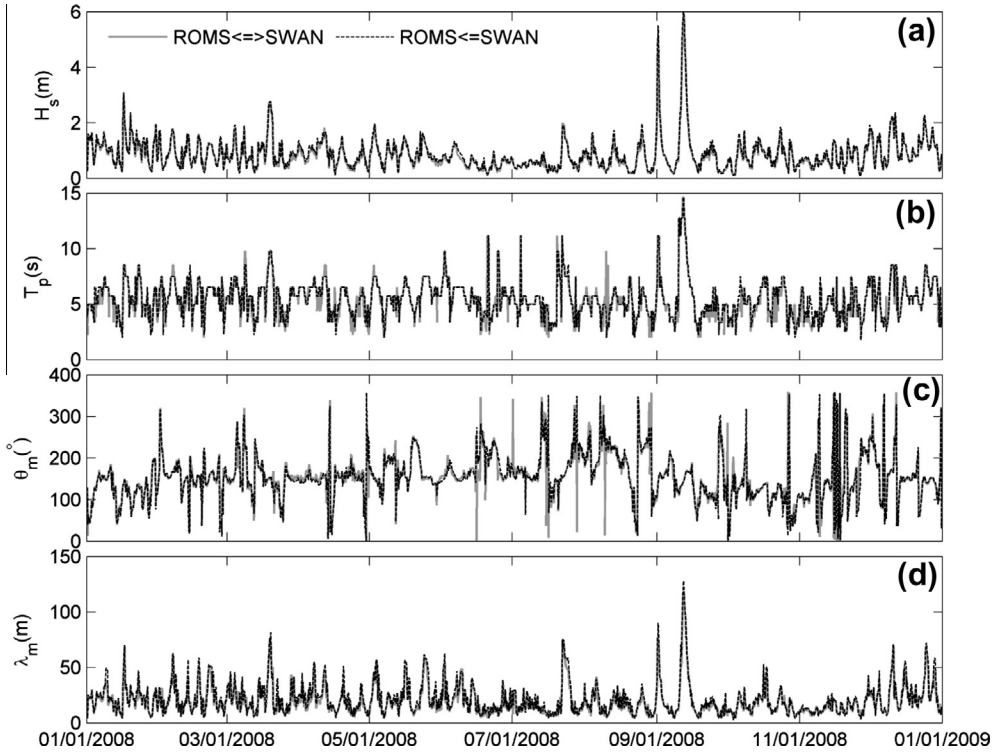

Fig. 5. . Comparison of (a) significant wave height, (b) surface peak wave period, (c) mean wave direction and (d) mean wave length between the two way coupled run (Two-Way-Couple, gray solid) and the one way coupled run (One-Way-Couple, black dashed) at the selected station C-09 (Fig. 1). The one way coupled run does not consider the feedback from the circulation model. Detailed configurations are summarized in Table 1.

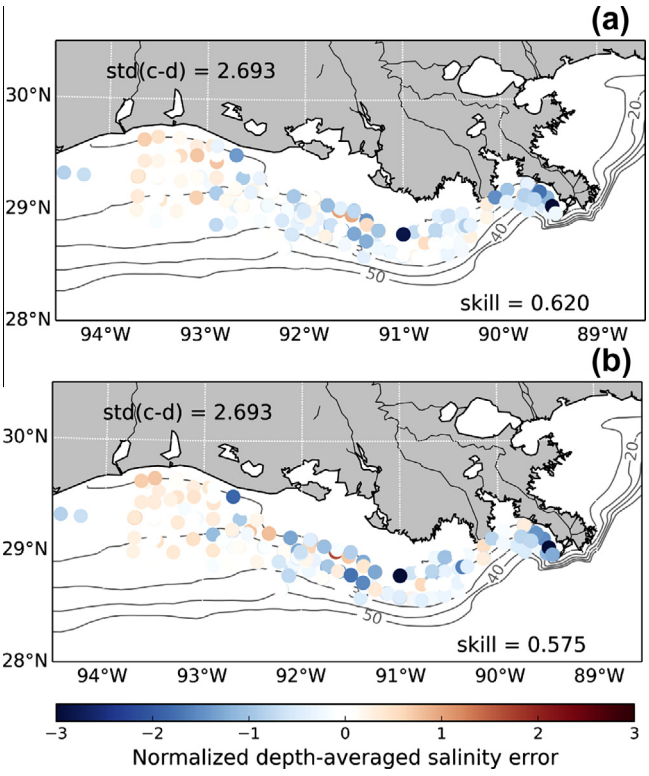

Fig. 6. Errors between the model simulated salinity and the MCH measurements averaged over the upper 50 m of water column and normalized by the standard deviation of the difference between the MCH measurements and climatology values for runs (a) without (Control) and (b) with (Two-Way-Couple) wave. Positive indicates the model overestimate the salinity. The standard deviation of the difference between the observed and climatological values and model skills are provided for each panel. 840 salinity profiles from 11 MCH cruises during 2005–2009 are used to estimate the model skill.

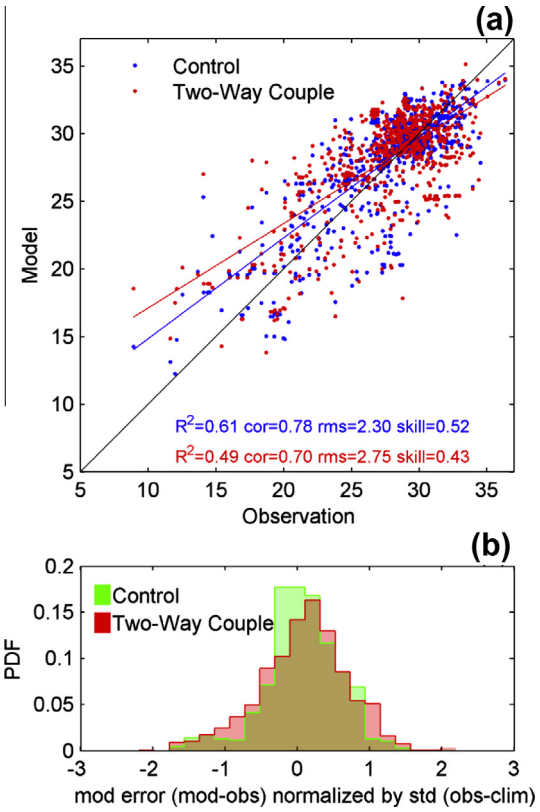

Fig. 7. (a) Comparison between model simulated surface salinity and the MCH observed surface salinity for 11 MCH collection periods during 2005–2009; (b) The probability distribution function of the errors between model simulated surface salinity and MCH measurements. The model error have been normalized by the stand deviation of the difference between the observed salinity and the climatological salinity.

A direct comparison between the observed and modeled salinity is shown in Fig. 7a. In general, the model simulation follows the observation relatively well, with the correlation of about 0.78 and the model skill of 0.52. Fig. 7b shows the error histograms for surface salinity simulation. The histogram represents point-by-point model error, normalized by the standard deviation of the observation relative to the climatology. The model error is nearly normally distributed. About 90% of the points have an error less than a standard deviation of the observations. Coupling waves to the ocean model lowers the salinity skill slightly (Figs. 6b and 7a) and spreads the error histograms to a broader space (Fig. 7b), but is statistically indistinguishable. A detailed discussion of wave effects on improvement of model skills is presented in Section 5.2.

The comparisons between model-simulated and observed salinity indicate the model simulates a realistic salinity field on the Texas–Louisiana shelf. Further validations of the hydrodynamic model are reported in Marta-Almeida et al. (2013) and Zhang et al. (submitted for publication). We conclude that the model can be used to identify wave effects on the dispersal of the Mississippi–Atchafalaya river plume.

4. Wave effects on stratification

Previous studies of wave effects on circulation have mainly focused on the modification of water level and mean currents by waves during extreme weather conditions, when the wave–current interactions are expected to be the strongest (e.g. Olabarrieta et al., 2012; Beardsley et al., 2013). However, we will show that the wave effects could also redistribute the freshwater and thus affect the stratification on seasonal cycles.

4.1. Wave effects on sea surface salinity

Wave effects on the circulation model are examined by plotting the difference of annual mean sea surface salinity between runs with (Two-Way-Couple) and without (Ctrl) wave effects (Fig. 8). As shown in Fig. 8, waves are apt to retain more freshwater to the inner shelf region, especially areas west of Terrebonne Bay and in the Chandeleur Sound. The annual mean surface salinity decreases by about 2 psu in the nearshore region in the case with waves, with the difference reducing offshore. The surface salinity west of the Mississippi Delta, i.e. salinity in the Louisiana Bight, is distinct from other regions. In contrast to the decreased surface salinity seen in the west, salinity in the Louisiana Bight increases by about 1 psu in the presence of waves. A small increase in sea surface salinity is also detected in the offshore side of the Louisiana shelf, i.e. region deeper than about 50 m, in water typically along the outer edge of the Mississippi–Atchafalaya plume. This pattern is consistent from year to year, with some modification due to interannual changes in river discharge and the wind field.

Wind-driven currents on the Texas–Louisiana shelf have distinct seasonal patterns and waves propagate in different directions during summer compared to non-summer periods (Fig. 4). The annual mean analysis does not consider the seasonal differences in plume position, that will be altered by interannual differences in wind and river discharge. Given the strong seasonal cycle that includes the reversal of the prevailing winds, seasonal patterns of surface salinity are analyzed. Fig. 9 shows the seasonal surface

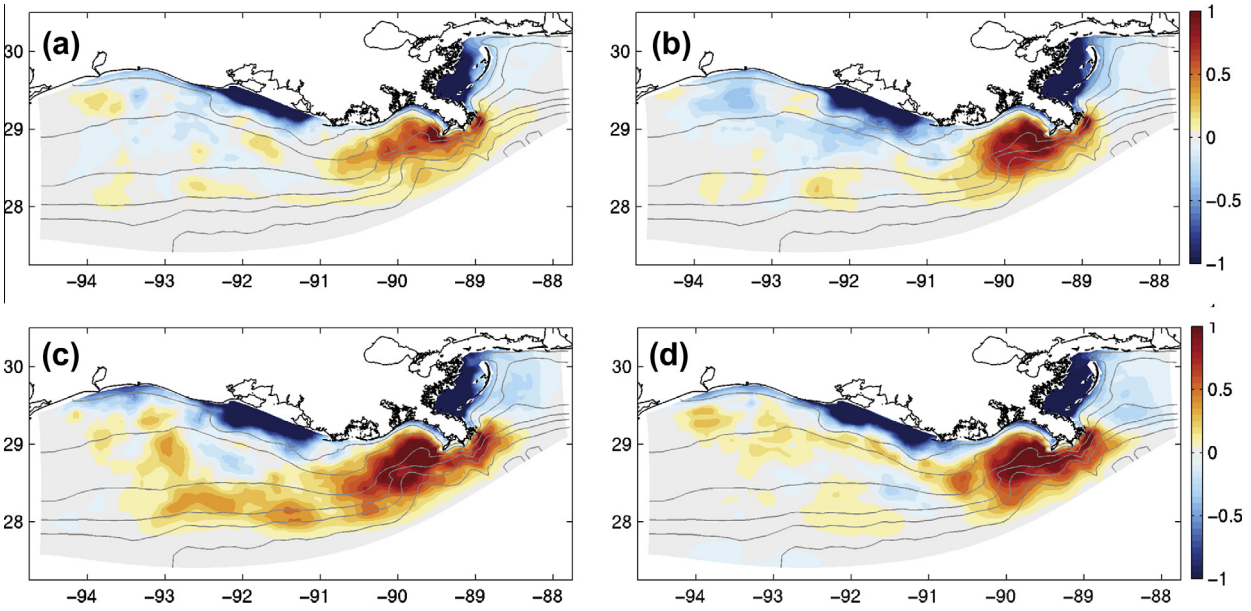

Fig. 8. Comparison of annual mean surface salinity difference between runs with (Two-Way-Couple) and without (Ctrl) waves at (a) 2006, (b) 2007, (c) 2008 and (d) 2009. Positive values indicate that the presence of waves has increased surface salinity.

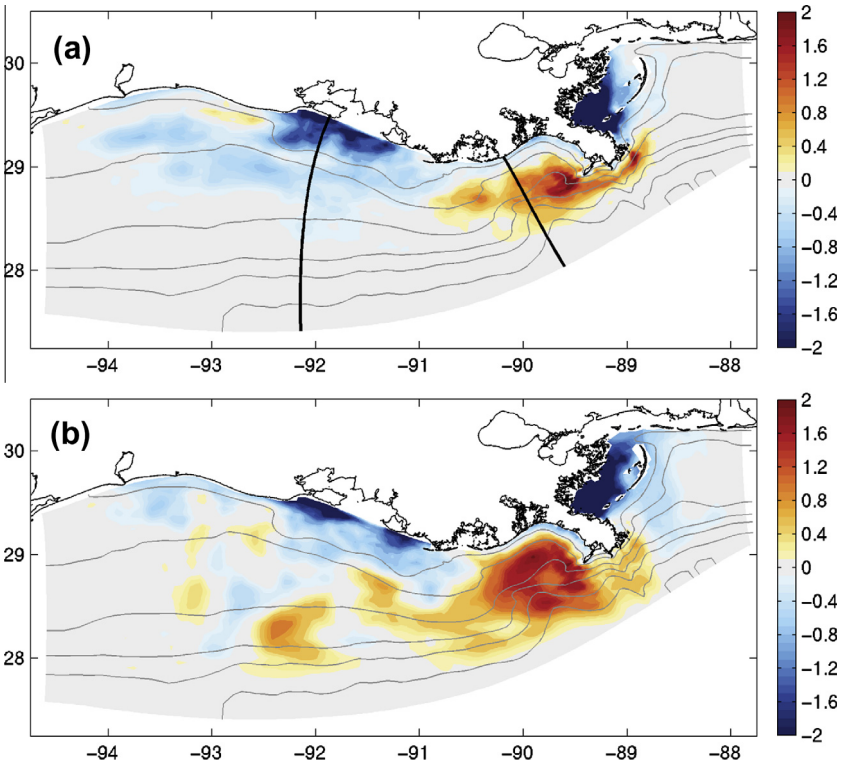

Fig. 9. Comparison of seasonal mean surface salinity difference between runs with (Two-Way-Couple) and without (Ctrl) waves at (a) December–January–February and (b) June–July–August during 2007. The thick solid lines in Fig. 9a mark the cross-sections analyzed in Fig. 10.

salinity difference between runs with and without waves in winter (December–January–February) and summer (June–July–August), 2007. The annual means are composites of the summer and winter patterns. In winter, the shelf is generally divided to western and eastern part approximately by the 91° W meridional line, with fresher water in the western part and saltier water in the eastern part in the case with waves. We will refer the western region as the Chenier shelf, extending roughly offshore from Sabine Lake to Vermilion Bay along the Gulf coast; the eastern part is referred to as the Louisiana Bight. Both regions are marked in Fig. 1. During summer when winds are upwelling favorable, the wind driven currents push the freshwater offshore. At the same time, wind induced mixing will entrain more saline water to the plume and reduce the salinity difference between the plume water and the ambient

water. In summer, the salinity difference between runs with and without waves in the nearshore region remains negative, meaning the case with waves is fresher, but the difference compared to winter in this same region is reduced considerably. The positive salinity anomalies in the Louisiana Bight also extend to a larger area in summer. The surface salinity in the middle shelf in winter (Fig. 9a) has switched from a negative to a positive difference, meaning that including waves tends to reduce surface salinity in winter and increase it in summer. We expect that this difference is caused by a complex interaction between the surface gravity wave field, summer wind forcing, and the active sub-mesoscale eddies.

4.2. Wave effects on stratification

As demonstrated in the previous section, wave processes cause a horizontal modification of the plume structure; there is a corresponding alteration of the vertical stratification. Fig. 10 shows the distribution of salinity differences between runs with (Two-Way-Couple) and without waves (Ctrl) in two cross-shelf profiles. The locations of the sections are shown in Fig. 9a, one across the Louisiana Bight, the other across the Chenier shelf. As shown in Fig. 10a, the annual mean salinity over the Chenier shelf decrease in regions shallower than 30 m, and exhibits an increase in near-surface waters offshore. Further comparisons are constructed for December–January–February and June–July–August. In winter, more freshwater is confined to the near coast region in the case with waves, and the salinity has decreased through the whole water column, with the maximum decrease near the coastline (Fig. 10c). During summer, fresher water is also trapped in the nearshore region, but to a lesser extent. The seawater becomes much saltier along the offshore front, by about 1 psu. Wave effects significantly reduce the summer stratification in the offshore region (Fig. 10e).

The eastern cross-section is located in the recirculating bugle region of the Mississippi river plume. The isohalines are nearly horizontal, especially in summer, unlike the horizontally stratified plume across the Chenier shelf. The annual mean salinity in a cross-shelf section shows an increase of salinity near the surface and a decrease beneath (Fig 10b), i.e., a decrease in vertical stratification. However, the seasonal patterns are quite different. In winter there is an increase in salinity through the whole water column, indicating that the freshwater is horizontally redistributed. In summer, the vertical salinity structure associated with the recirculating plume is much more pronounced. The surface salinity increases while the lower layer decreases, in the same sense as the annual mean, when wave effects are included, again suggesting the freshwater is vertically redistributed.

The seasonal stratification is represented by surface to bottom salinity differences, and is plotted as a function of total water depth (Fig. 11). The shelf is again divided roughly into the Louisiana Bight and the Chenier shelf by the 91° W meridional line, and the stratification corresponding to different depths is averaged in each region separately. Data east of the Mississippi Delta is not considered when averaging. As shown in Fig. 11, the Louisiana Bight has the largest surface-bottom salinity difference of about 15 psu in spring (Fig. 11b) and lowest of about 3 psu in fall (Fig. 11d). The stratification on Chenier shelf is weaker than the bulge region, with the maximum of about 6 psu in spring (Fig. 11b) and ~1.5 psu in other seasons. With the inclusion of wave effects, the stratification in the inner shelf (<20 m) is weakened all through the year over both the Louisiana Bight and Chenier shelf. That is to say, although waves trap more freshwater to the inner shelf region, enhanced bottom friction and wave mixing continue to reduce stratification there. Stratification over the mid-shelf (20–50 m) is different between the Louisiana Bight and the Chenier shelf. The mid-shelf stratification on the Chenier shelf is

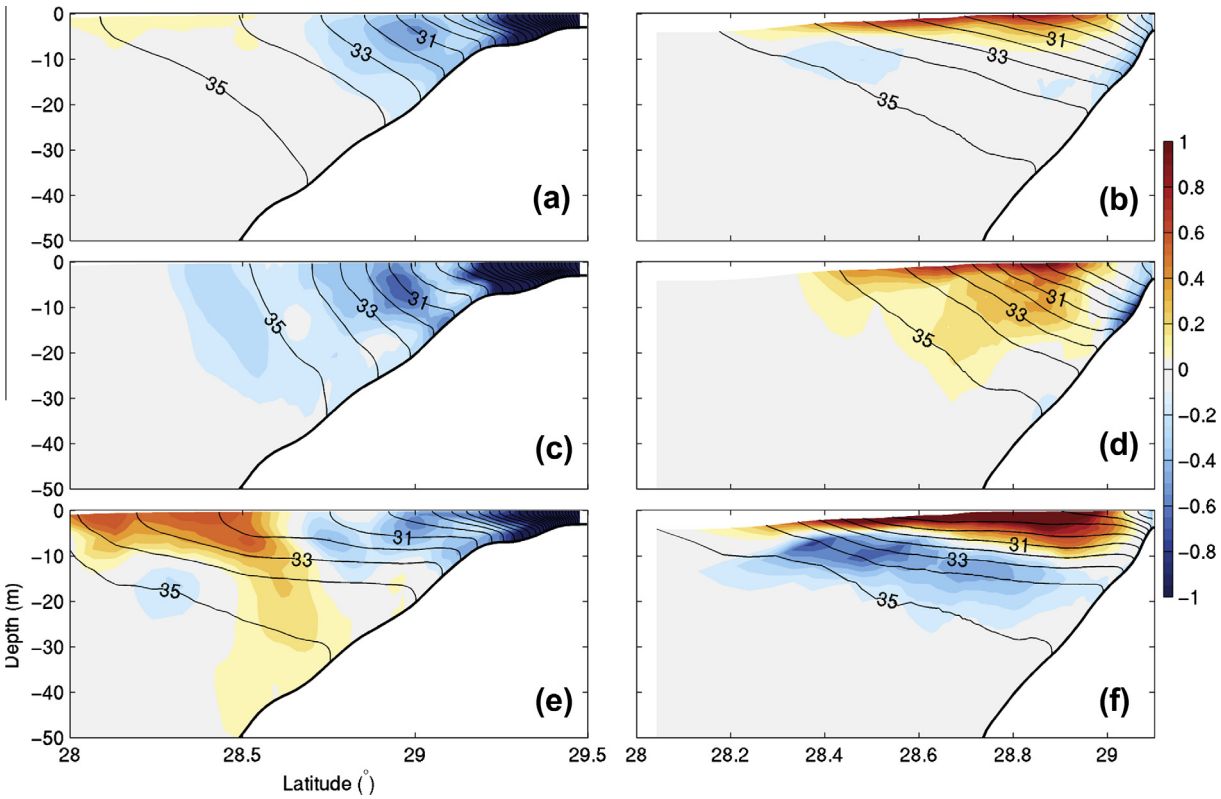

Fig. 10. Distributions of salinity difference between the coupled run (Two-Way-Couple) and the control run (Ctrl) in two cross-shelf sections averaged over (a, b) a whole year, (c, d) DJF and (e, f) JJA during 2007. The left (right) panel is the west (east) section shown in Fig. 9a.

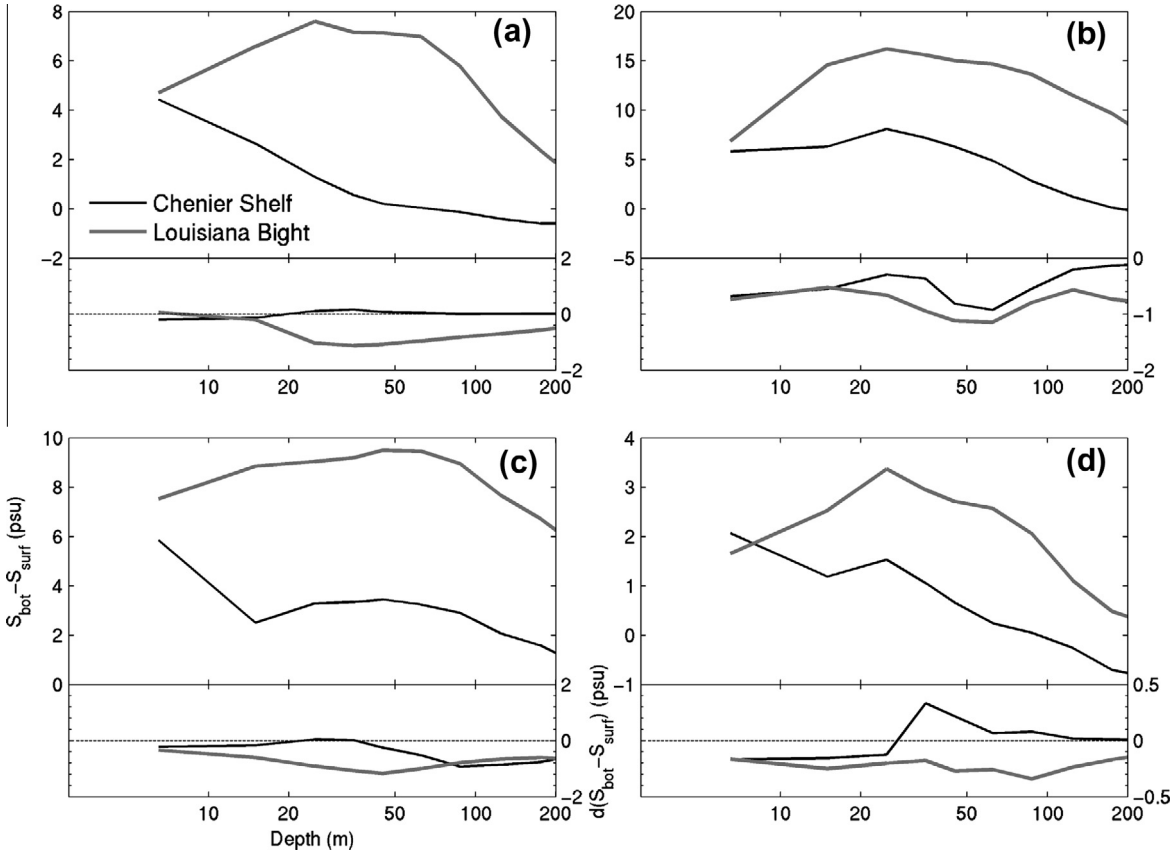

Fig. 11. Stratification representing by the surface-bottom salinity difference (upper panel) in the control run (Ctrl) and its difference (lower panel) to the run with waves (Two-Way-Couple) as a function of depth at (a) February, (b) May, (c) August and (d) November during 2007. The shelf is divided to the Louisiana Bight and the Chenier Shelf by approximately the −91° meridional line, and stratification corresponding to different depth is averaged in each region. Note that the range of the *y*-axis is different for the four sub-panels.

weakened in spring and summer, but can be slightly enhanced through fall and winter (Fig. 11). As revealed by the cross-shelf distribution of salinity in Fig. 10c and e, the surface salinity of the mid-shelf on Chenier shelf decreases in winter and increases in summer, which is the cause for the varied stratification. In the Louisiana Bight, waves reduce the stratification through the whole year; the increased surface salinity (Fig. 10b and d) is responsible for the weakened stratification there.

4.3. Circulation pattern modification by waves

One of the primary drivers for tracer field modification is advective tracer fluxes depending on the circulation pattern. This circulation pattern gets modified due to the presence of wave forcing in the form of enhanced bottom stress, surface mixing and additional momentum flux through vortex force. Fig. 12a shows the difference of the annual mean depth-averaged Lagrangian mean flow between runs with (Two-Way-Couple) and without (Ctrl) waves. As shown in Fig. 12a, the Louisiana Bight and the inner part of Chenier shelf identify two regions with strong circulation modifications, indicating strong wave–current interactions there. Coupling waves to the ocean model retards the Lagrangian mean flow on the inner part of Chenier shelf by about 0.02–0.04 m/s, 10–20% of its original value. Changes in Louisiana Bight are also remarkable but are relatively chaotic, with strengthened and weakened current accompanied each other. Such modifications to the circulation pattern are apt to trap more freshwater to the inner part of Chenier shelf and arrest its offshore dispersal, consistent with modifications to the surface salinity (Fig. 8). However, it is important to point out that changes in salinity field cannot be attributed to changes in circulation pattern directly, since changes in the tracer field will feedback on the flow field, especially in the presence of river plumes where the river buoyancy is one of the primary drivers of the current.

There are previous studies showing that surface waves can decrease the ocean current by enhancing the bed stress (e.g. Davies and Lawrence, 1995; Signell and List, 1997) and increase the ocean current by transferring wave momentum (e.g. Perrie et al., 2003). To gain some insights, we have conducted three additional runs to investigate the effects of different wave processes (see Table 1 for configuration). As shown in Fig. 12b–d, the weakened mean flow in the inner shelf is mainly due to the enhanced bottom stress, which tends to retard the current (Fig. 12c). Changes in Louisiana Bight are relatively chaotic, however, are mainly caused by the excessive wave mixing and wave vortex forces (Fig. 12b and d). The difference on the mid- and outer-shelf in all three cases looks like random noises. It is expected since these are areas where nonlinear instability exists due to interaction of the Mississippi–Atchafalaya river plume front and the offshore eddies (Hetland and DiMarco, 2012; Marta-Almeida et al., 2013). The nonlinearity renders the flow field chaotic through the role of eddies.

In the absence of wave–current interactions, the dominant momentum balance in both the cross- and alongshore direction occurs between the pressure gradient, the Coriolis force and the vertical stress divergence; the horizontal and vertical advections tend to cancel each other and play a secondary role (not shown). This is consistent with a previous view of inner-shelf momentum balance over the Texas–Louisiana shelf (Zhang et al., 2014). Adding waves change all momentum terms accordingly, especially in the

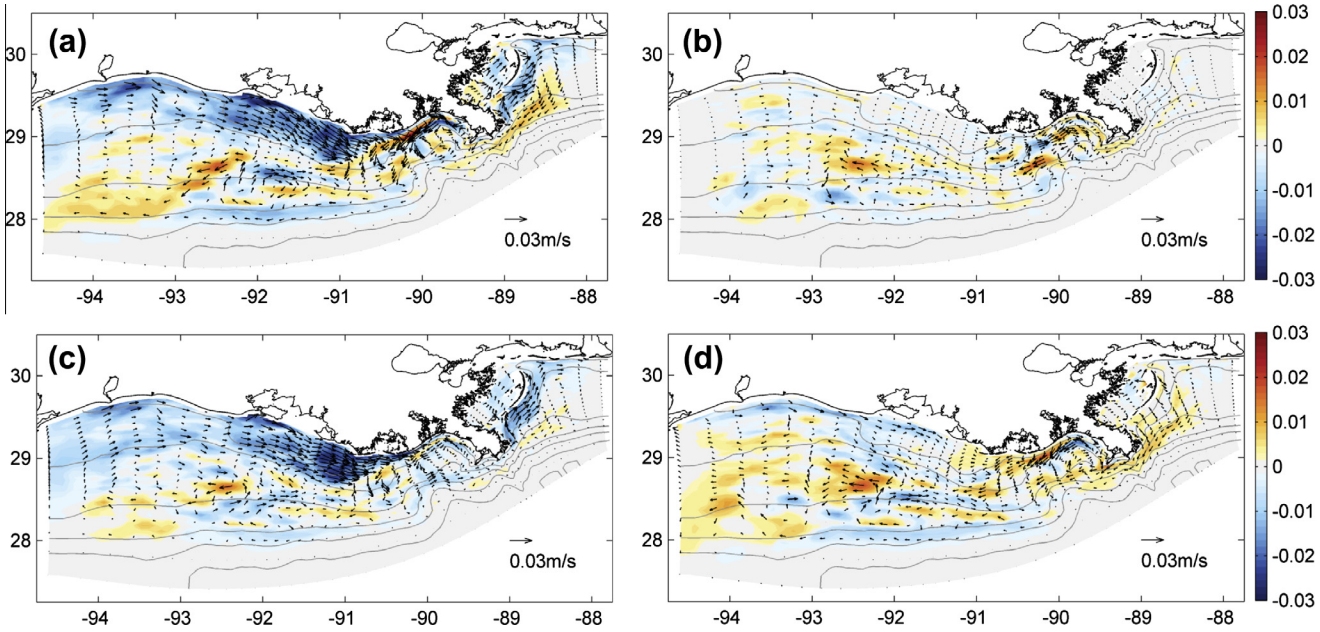

Fig. 12. Difference of annual mean depth-averaged Lagrangian mean flows (m/s) between runs (a) Two-Way-Couple, (b) Couple TKE, (c) Couple-BBL, (d) Couple-VF and the control run during 2007. Arrows show changes in the mean current vector. Colors show changes in the magnitude of the mean current, with positive value indicating the current is strengthened and vice versa.

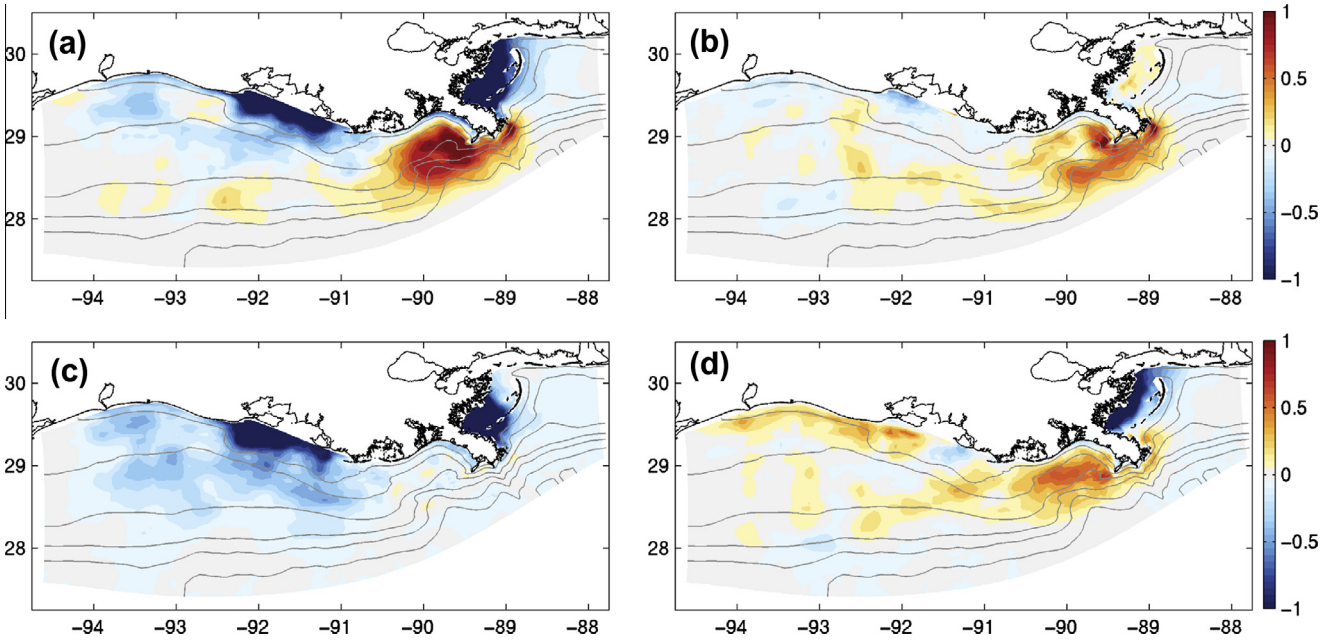

Fig. 13. Difference of annual mean surface salinity between runs (a) Two-Way-Couple, (b) Couple-TKE, (c) Couple-BBL, (d) Couple-VF and the control run (Ctrl) during 2007.

upper water column, but the main balance is still between the pressure gradient, the Coriolis force and the vertical stress divergence. The maximum changes are to the pressure gradient and the Coriolis force, suggesting the changes in stratification, surface elevation and current velocity, as is indicated by the modification to the circulation pattern (Fig. 12). The momentum balance presented here is different from the balance in the surf zone, which is not resolved in the present model, where the wave forcing terms are dominant (see e.g. Uchiyama et al., 2010).

4.4. Role of wave enhanced bottom stress

Given the distinct effects of different wave processes on circulations, it is useful to show how different wave processes affect the plume structure. In addition to surface salinity, the freshwater thickness is also investigated, which contains the vertical information of the plume. The freshwater thickness is defined as the integral of the fresh water anomaly over the vertical water column:

$$h_f = \int_{-H}^{\eta} \frac{S_0 - S}{S_0} dz \tag{2}$$

The reference salinity, S_0, used in the calculation of the freshwater thickness is 36 psu. Different reference salinity could be used but that makes no difference to the analysis results since we are focusing on the changes in freshwater thickness.

Fig. 13 shows the annual mean surface salinity difference between the fully- and partly-coupled runs as compared with the control run without waves. The composite of the three partly cou-

pled runs resembles the fully coupled run surprisingly well, suggesting there is little interaction between the three wave effects. The decrease in surface salinity in the inner and middle shelf is mainly due to the enhanced bottom stress. The enhancement of the bottom roughness and the resultant bottom stress is confined to regions shallower than 50 m (Fig. 15a and c). Its effects are dominant over the Chenier shelf and the Chandeleur Sound, but play only a minor role in the Louisiana Bight, where the bottom slope is steeper (Fig. 13c).

The Mississippi river plume disperses over a steep narrow shelf and behaves as a surface-trapped plume in the Louisiana Bight, and is not strongly influenced by interaction with the bottom (Yankovsky and Chapman, 1997). Thus the surface salinity shows little difference between runs with and without wave bottom boundary in the Louisiana Bight (Fig. 13c). Fig. 14 shows the difference of annual mean freshwater thickness between the fully- and partly-coupled runs as compared with the control run. As expected, the freshwater thickness of run Couple-BBL reveals only slight variations in the Louisiana Bight (Fig. 14c).

In contrast to the steep Louisiana Bight, the buoyancy driven current over the Chenier shelf interacts strongly with the bathymetry (Zhang et al., 2014). Such an interaction might be altered by the presence of waves. As revealed by the model simulation, presence of waves increases the effective bottom roughness felt by the mean flow; the bottom roughness length in the presence of wave increases by a factor of 2–20 compared to 0.001 m (Fig. 15a). Taking a reference height of 0.1 m ($z = 0.1$ m), this corresponds to an increase in the drag coefficient by a factor of about 1.5–8. In response to the increased bottom drag, however, the simulated bottom currents are reduced in the inner shelf region by about 20–60 percent (Fig. 15b). Since the bottom stress is proportional to the bottom drag and the square of the bottom velocity, the bottom stress increases by about 20–60% instead of factor of 1.5–8 (Fig. 15c).

In fact, wave induced enhancement of the bottom stress encountered by currents has been studied both theoretically (Christoffersen and Jonsson, 1985) and experimentally (Gross et al., 1992; Mathisen and Madsen, 1996). Its effects in retarding the bottom current have also been addressed by many previous studies (e.g., Davies and Lawrence, 1995; Signell and List, 1997). However, few of them linked it to the tracer dynamics. Chao and Boicourt (1986) pointed out that the development of buoyancy current could be trapped by enhanced bottom friction. In the absence of bottom friction, the intrusion speed of a buoyancy-driven bore is significantly accelerated and highly nonlinear, which is consistent to our results here. The wave enhanced bottom stress dominates the redistribution of the freshwater in the shelf region with a gentler bottom slope, where the Mississippi–Atchafalaya plume intersects the bottom. Inclusion of waves in the bottom boundary layer is apt to retard the currents (Fig. 15c) and retain more freshwater to the nearshore region (Fig. 13c). The accumulation of freshwater increases the freshwater thickness correspondingly (Fig. 14c). In general, with water depth more than 50 m the effect of wave enhanced friction is not significant.

4.5. Roles of wave mixing and 3-D wave forces

The increase of surface salinity in the Louisiana Bight is mainly due to the surface enhanced mixing and the 3-D wave momentum (Fig. 13b and d). Wave breaking induced dissipation leads to mixing of momentum in the water column (Carniel et al., 2009). If injection of TKE due to breaking waves is considered, the TKE profile is modified in the surface layer to a depth proportional to the wave height. The vertical eddy viscosity keeps a parabolic profile, but it is greatly enhanced near the surface (not shown). The enhanced vertical eddy viscosity will increase mixing with the ambient water. The plume in the Louisiana Bight is thin compared with other regions of the plume; therefore the effects due to wave mixing there are largest.

The effects of surface wave mixing and the excessive 3-D wave forces have similar patterns with each other (Fig. 13b and d), however, the intrinsic physical processes are different. Wave mixing causes an exchange of turbulence vertically and its effects are then spread out by the lateral mixing and advection. The 3-D wave forces, on the other hand, could redistribute the momentum directly, both horizontally and vertically. These different effects can be seen in the distribution of freshwater thickness (Fig. 14). The increased surface salinity in the Louisiana Bight in the run Couple-TKE (Fig. 13b) corresponds to an increase of freshwater thickness (Fig. 14b). Conversely, the increased surface salinity of run

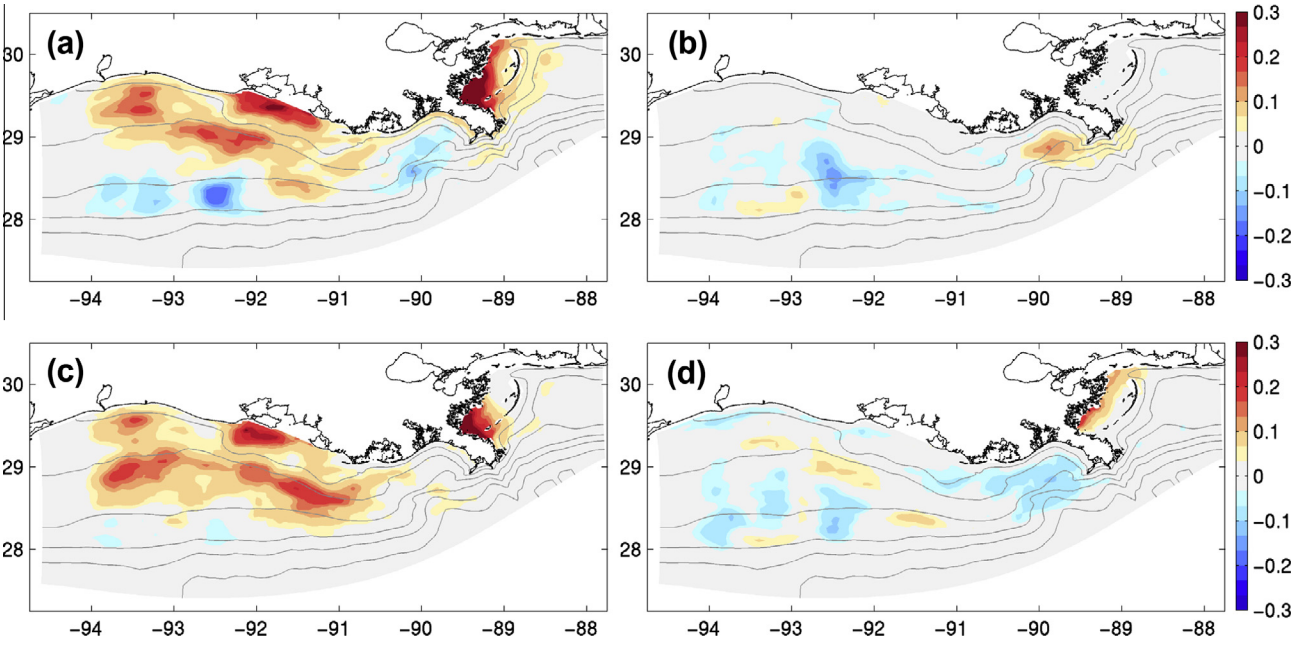

Fig. 14. Difference of annual mean freshwater thickness (m) between runs (a) Two-Way-Couple, (b) Couple-TKE, (c) Couple-BBL, (d) Couple-VF and the control run (Ctrl) during 2007.

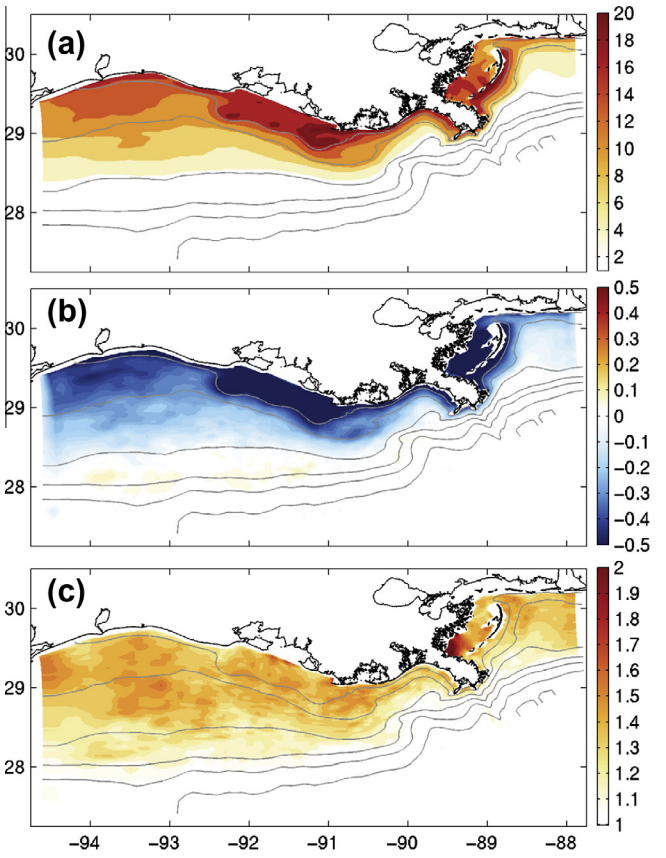

Fig. 15. The ratio of model simulated (a) bottom roughness length scale enhancement due to waves; (b) bottom current reduction due to waves; and (c) bottom stress enhancement due to waves between runs with (Two-Way Couple) and without (Ctrl) wave bottom boundary layer during 2007.

Couple-VF (Fig. 13d) corresponds to a decrease of freshwater thickness (Fig. 14d) in the Louisiana Bight. That is to say, wave mixing in the run Couple-TKE deepens the surface mixed layer, increasing the salinity near the surface and decreasing the salinity beneath it, and the overall freshwater thickness increases as more freshwater is introduced. The increased surface salinity in run Couple-VF (Fig. 13d), on the other hand, is mainly due to the redistribution of freshwater horizontally, thus the increased surface salinity corresponds to decreased freshwater thickness (Fig. 14d). These different effects can also be seen in cross shelf salinity distributions in the fully coupled run (Fig. 10d and f). The winter season is characterized by a net water column increase in salinity (Fig. 10d), while in summer the increased surface salinity is accompanied by a decrease in salinity below (Fig. 10f).

5. Discussion

5.1. Different wave effects dominate different plume regions

One notable result from the fully- and partly-coupled runs is the relatively weak interaction between three different wave effects. This is reasonable considering their original sources. The wave bottom stress, originating from the bottom boundary layer, occurs primarily in shallow waters. The surface wave mixing and the 3-D wave forces, on the other hand, are generally surface intensified. The interaction between them can only be significant when the surface and bottom boundary layers overlap. Thus, the shallow inner- and mid-shelf regions might be identified as potential regions where the various wave effects interact. However, the shallow regions are generally well-mixed, by both wind and shear mixing. Therefore, the altering of the water column stratification by additional wave mixing may be less pronounced, as the water column has already been mixed. The different wave effects thus tend to divide the Texas–Louisiana shelf into two dynamically distinct regions: the Louisiana Bight and the Chenier shelf, which are dominated by different wave processes, respectively (Figs. 8 and 13).

Previous studies have also identified differences in these two regions. Hetland and DiMarco (2008) found the mechanisms controlling the hypoxia over the Louisiana Bight and the Chenier shelf were distinct and attributed them to different dynamically characteristics of the Mississippi and Atchafalaya river plume. Salisbury et al. (2004) found that while optical properties were correlated with the river discharge in the Louisiana Bight, they were correlated with the wind over the Chenier shelf. Addition of waves further identifies these two dynamically distinct regions, which will in turn affect the formation and evolution of stratification over the Texas–Louisiana shelf.

The Louisiana Bight is dominated by the additional 3-D wave forces and wave mixing. Heavy freshwater imported from the Mississippi river forms a thin recirculating bulge in the Louisiana Bight. This recirculating bulge is associated with relatively strong currents (Zhang et al., 2012), and thus a potential area of strong wave–current interaction. Correspondingly, excessive wave momentum generates salient salinity difference in the Louisiana Bight compared to other regions (Fig. 13d), as the circulation there is altered by the excessive wave forces (Fig. 12d). The parameterized wave mixing is proportional to the significant wave height, which is comparable to the plume thickness in Louisiana Bight. Thus mixing may be more efficient in the Louisiana Bight compared to the Chenier shelf, where the plume is much thicker.

In contrast to the Louisiana Bight, the Chenier shelf is dominated by the enhanced bottom stress; the surface intensified wave turbulence and 3-D wave momentum have lower efficiency in this area. The wave enhanced bottom stress retains more freshwater in the inner shelf by decreasing currents, potentially increasing the filling and flushing time of fresh water over the Texas–Louisiana shelf. We have estimated the changes of freshwater volume in the whole model domain with the inclusion of wave enhanced bottom friction. More freshwater is confined within the model domain compared to the run without waves. Estimation shows that the filling time ($dV_{freshwater}/Q_{river}$) is about 2–6 days longer with waves included, depending on the river discharge.

The idea of different regions being affected by different process may be useful in simplifying the process of including waves in a hydrodynamic model, because it may only be necessary to include a subset of the three wave–current processes. For example, when simulating shelf dynamics on a broad-slope shelf, the effects of wave bottom stress should be considered the first priority. Inclusion of wave mixing will be essential in many surface trapped plumes, e.g. the Columbia River, the Merrimack River, during high river discharge seasons, or any time the injection depth of wave mixing is similar to the plume thickness. Also, future observations of wave mixing would be more useful in the Louisiana Bight, where the effect of wave mixing can be measured, otherwise wave mixing effects might be obscured by other processes. The results presented here might also be helpful in understanding many phenomena over the Texas–Louisiana shelf. For example, the sediment plume over the Mississippi river bulge region is more likely due to advection and re-entrainment, while the bottom erosion and re-suspension would be dominant around the Atchafalaya Bay, consistent with the findings of Salisbury et al. (2004).

5.2. Wave effects on model skill

As revealed in Section 4, including of wave effects alters the stratification and distribution of freshwater over the shelf. Stratifi-

cation is not necessarily weakened; accumulated freshwater on Chenier inner-shelf corresponds to an enhanced stratification during fall and winter (Fig. 11a and d). When winds are stronger or persist longer during summer, other processes like wave mixing dominate over the horizontal redistribution of freshwater. The stratification, instead of being strengthened, is weakened (Fig. 11b and c). With the addition of wave mixing, Gerbi et al. (2013) also showed that the stratification is enhanced in the plume center, which is counter-intuitive. This may be because the addition of waves has modified the freshwater filling and flushing time and thus the plume structure, which is consistent with our results here.

Though changes to stratification are pronounced in terms of monthly and annual means, the coupled model shows no improvement in terms of salinity skill. As shown in Fig. 6b, the model skill in the coupled run is even slightly lower than the control run. This is mainly because the RMS error of the coupled run increases slightly compared to the run without waves, indicating the system is more energetic. The comparison of the surface salinity shows that the model has a tendency to overestimate the low salinity class and underestimate the high salinity class (Fig. 7a). Coupling waves to the ocean model was expected to improve this since more freshwater was arrested to the nearshore region, i.e. low salinity classes; but we saw no evidence from Fig. 7a. The error histograms show no systemic bias when adding waves (Fig. 7b). However, the histogram is broadened when coupling waves, suggesting the model with waves included is more dynamically active, but not distinguishably better or worse than the model without waves based on available observations.

Hetland and Dimarco (2012) assessed model skill over the Texas–Louisiana shelf and found that the model, without waves, is able to reproduce the broad-scale features of salinity distributions over the shelf faithfully. However, the model has difficulty in reproducing the small spatial and temporal scale energetic features. These features are chaotic, with a variability of a similar magnitude to the broader-scale changes to salinity over the shelf (Marta-Almeida et al., 2013). As such, it is not surprising that we are not able to determine if including waves improves the simulation based on a comparison with observations. The wave-induced modifications to the salinity field are smaller than the noise inherent in the observations due to the small-scale, energetic features over the shelf. In addition, the absence of detailed wind structure might mis-place the small-scale eddies, which might obscure the skill analysis. Sclavo et al. (2013) found that the coupled wave-ocean models reproduced better small-scale characteristics in Adriatic Sea than the ocean model itself, by adopting high resolution wind. The performance of the coupled modeling system driven by high temporal and spatial resolution wind field will be evaluated over the Texas–Louisiana shelf in future studies.

5.3. Feasibility of one way coupling on seasonal scale

We have demonstrated that the effects of the circulation model on the wave field are relatively weak in Section 3.1. The effects of the altered wave field due to including a varied current field and water level are less than 10% of the effects due to the wave field simulated without the effects of shelf currents. We have compared the difference of the annual mean surface salinity distribution between the one-way and two way coupled simulations. The differences are generally less than 0.2 psu, 5% less than its seasonal variation (not shown). More importantly, the differences are randomly distributed. This means that although the maximum instantaneous difference between the one-way and two way coupled simulations might be large, for example, a tiny shift in the plume front cause a large salinity bias nearby, its cumulative effect introduce no system bias to the seasonal salinity distribution. The temporal average acts as a filter to smooth out the small-scale variability both temporally and spatially. So if the broad-spatial scale and seasonal temporal scale are of interest, the two-way coupling effects might be neglected. This generally allows using a simplified one-way coupled model to simulate the wave effects on the seasonal shelf-scale circulation and stratification. If a simulation of wave conditions already exists on this scale, the wave parameters could be used to estimate the wave effects on the ocean current model without running an expensive coupled wave–current model. Also, as discussed above, if the seasonal shelf-scale is of interest, it may be possible to only include certain wave effects. Thus some properties of the wave field may not need to be calculated; certain parameterization could be used to examine the wave effects in terms of wave mixing (e.g. Craig and Banner, 1994) and wave bottom stress (e.g. Signell and List, 1997). However, if we are interested in instantaneous results in extreme weather conditions rather than the seasonal means, the detailed wind structure and the two-way coupled current–wave interactions may need to be considered.

6. Conclusion

We have configured the COAWST modeling system to study wave–current interactions over the Texas–Louisiana shelf. The modeling system is driven by realistic wave and current conditions at the open boundaries and 1-D wind measured from a nearby meteorological station, taking advantage of its high temporal resolution. Comparison with observations demonstrates that the modeling system is able to reproduce the wave and salinity fields. Wave characteristics are first investigated from the SWAN wave model. Winds and waves over the Texas–Louisiana shelf have good correspondence with each other, indicating that waves over the Texas–Louisiana shelf are dominated by locally generated wind seas with periods mostly less than 8 s, that propagate in the same direction as the wind. Comparative runs with and without shelf currents provided from the circulation model have been conducted to discern the effects of water level and currents on wave fields. Relatively weak effects were found for the circulation model on the wave fields and the relative differences are generally less than 10%. Such changes in wave characteristics play a minor role when investigating the seasonal salinity distribution. Given this, if seasonal scale is of interest, one way coupled models could be adopted to study the wave effects on the circulation model, taking advantage of existing wave products. A recent study in Adriatic Sea showed that the effects of wave–current interaction on waves might be small even during a strong storm event, depending on the wind direction and current velocity (Benetazzo et al., 2013). The feasibility of one-way coupling to other temporal and spatial scales remains an open question for future studies.

Including the effects of waves redistributes the freshwater both vertically and horizontally. Two dynamically distinct regions are identified: the Chenier shelf and the Louisiana Bight. Including waves in the simulation causes more freshwater to be trapped in the inner part of Chenier shelf, decreasing the surface salinity and increasing the freshwater thickness. Wave enhanced bottom stress dominates the redistribution of freshwater in this area. Bottom roughness and wave–current velocities determine the bottom stress, which retards the currents. Stratification on Chenier shelf could either be intensified or weakened, depending on the competition between the horizontal advection and the vertical mixing processes.

The Louisiana Bight is identified as another dynamical region. The recirculating plume is thin there and is associated with relatively strong currents. Mixing due to wave breaking and the 3-D wave vortex forces are dominant in this area; both are effective

in decreasing the surface salinity and weakening the stratification. However, the two forces work differently; wave breaking mixes the water column – a vertical process, while the 3-D wave force mainly redistributes the plume laterally – a horizontal process.

The interaction of three different wave effects is relatively weak. The composite of the process-oriented runs resembles the fully coupled runs very well. This allows studying the wave effects separately and potentially only including a subset of the wave processes in a domain known to be primarily affected by one wave process.

Although wave induced exchange between the surf zone and the inner shelf also affects the plume dynamics, this paper has focused on the shelf scale processes and interactions between the inner- and outer-shelf. In the future it would be interesting to identify the physical processes controlling the exchange between the surf zone and the inner shelf, as well as the internal circulation and dynamics. It would also be interesting to show how waves affect the circulation and tracer dynamics at the event time scale.

Acknowledgements

We are grateful to three anonymous reviewers for their insightful comments. This study is funded by the Texas General Land Office through TGLO TABS Modeling Effort (Award No. 08-054-000-1146) and TGLO Improving Hydrodynamic Predictions (Award No. 10-096-000-3927). Z. R. acknowledges support by NSF of China project 41406008.

References

Ardhuin, F., Jenkins, A.D., Belibassakis, K.A., 2008. Comments on the three dimensional current and surface wave equations. J. Phys. Oceanogr. 38, 1340–1350.

Ardhuin, F., Roland, A., Dumas, F., Bennis, A.-C., Sentchev, A., Forget, P., Wolf, J., Girard, F., Qsuna, P., Benoit, M., 2012. Numerical wave modeling in conditions with strong currents: dissipation, refraction, and relative wind. J. Phys. Oceanogr. 42, 2101–2120.

Barth, A., Alvera-Azcarate, A., Weisberg, R.H., 2008. Benefit of nesting a regional model into a large scale ocean model instead of climatology. application to the West Florida Shelf. Cont. Shelf Res. 28, 561–573.

Beardsley, R.C., Chen, C., Xu, Q., 2013. Coastal flooding in Scituate (MA): a FVCOM study of the 27 December 2010 nor'easter. J. Geophys. Res. 118, 1–16.

Benetazzo, A., Carniel, S., Sclavo, M., Bergamasco, A., 2013. Wave–current interaction: effects of the wave field in a semi-enclosed basin. Ocean Modell. 70, 152–165.

Bennis, A., Ardhuin, F., Dumas, F., 2011. On the coupling of wave and three-dimensional circulation models: choice of theoretical framework, practical implementation and adiabatic tests. Ocean Modell. 40 (3–4), 260–272.

Booij, N., Ris, R., Holthuijsen, L., 1999. A third generation wave model for coastal regions. I- model description and validation. J. Geophys. Res. 104 (C4), 7649–7666.

Carniel, S., Warner, J.C., Chiggiato, J., Sclavo, M., 2009. Investigating the impact of surface wave breaking on modeling the trajectories of drifters in the northern Adriatic Sea during a wind-storm event. Ocean Modell. 30 (2–3), 225–239.

Chao, S.Y., Boicourt, W.C., 1986. Onset of estuarine plumes. J. Phys. Oceanogr. 16, 2137–2149.

Chapman, D., 1985. Numerical treatment of cross-shelf open boundaries in a barotropic coastal ocean model. J. Phys. Oceanogr. 15, 1060–1075.

Charnock, H., 1955. Wind stress on a water surface. Q. J. R. Meteorol. Soc. 81, 639–640.

Cho, K., Reid, R.O., Nowlin Jr, W.D., 1998. Objectively mapped stream function fields on the Texas–Louisiana shelf based on 32 months of moored current meter data. J. Geophys. Res. 103, 10377–10390.

Christoffersen, J.B., Jonsson, I.G., 1985. Bed friction and dissipation in a combined current and wave motion. Ocean Eng. 12 (5), 387–423.

Craig, P.D., Banner, M.L., 1994. Modeling wave enhanced turbulence in the ocean surface layer. J. Phys. Oceanogr. 24, 2546–2559.

da Silva, A.M., Young-Molling, C.C., Levitus, S., 1994. Altas of Surface Marine Data 1994 Volume 1: Algorithms and Procedures. NOAA Altas NESDIS 6 Technical Report. U. S. Gov. Printing Office, Washington, DC.

Davies, A.M., Lawrence, J., 1995. Modeling the effects of wave–current interaction on the three-dimensional wind-driven circulation on the eastern Irish Sea. J. Phys. Oceanogr. 25, 29–45.

DiMarco, S.F., Chapman, P., Walker, N., Hetland, R.D., 2010. Does local topography control hypoxia on the eastern Texas–Louisiana Shelf? J. Mar. Syst. 80, 25–35.

Etter, P.C., Howard, M.K., Cochrane, J.D., 2004. Heat and freshwater budgets of the Texas–Louisiana shelf. J. Geophys. Res. 109, C02024. http://dx.doi.org/10.1029/2003JC001820.

Fan, Y., Glinis, I., Hara, T., 2009. The effect of wind–wave–current interaction on air-sea momentum fluxes and ocean response in tropical cyclones. J. Phys. Oceanogr. 39, 1019–1034.

Feddersen, F., Trowbridge, J.H., 2005. The effect of wave breaking on surf zone turbulence and alongshore currents: a modeling study. J. Phys. Oceanogr. 35, 2187–2203.

Fennel, K., Hetland, R., Feng, Y., DiMarco, S., 2011. A coupled physical-biological model of the Northern Gulf of Mexico shelf: model description, validation and analysis of phytoplankton variability. Biogeoscience 8, 1881–1899.

Flather, R., 1976. A tidal model of the northwest European continental shelf. Mem. Soc. R. Sci. Liege 10 (6), 141–164.

Gerbi, G.P., Chant, R.J., Wilkin, J.L., 2013. Breaking surface wave effects on river plume dynamics during upwelling-favorable winds. J. Phys. Oceanogr. 43, 1959–1980.

Grant, W.D., Madsen, O.S., 1978. Bottom friction under waves in the presence of a weak current. NOAA Technical Memorandum ERL MESA, p. 131.

Gross, T.F., Isley, A.E., Sherwood, C.R., 1992. Estimation of stress and bed roughness during storms on the North California Shelf. Cont. Shelf Res. 12 (2–3), 389–413.

Haidvogel, D.B., Arango, H., Hedstrom, K., Beckmann, A., Malanotte-Rizzoli, P., Shchepetkin, A., 2000. Model evaluation experiments in the North Atlantic Basin: simulations in nonlinear terrain-following coordinates. Dyn. Atmos. Oceans 32, 239–281.

Hetland, R.D., 2006. Event driven model skill assessment. Ocean Modell. 11 (1–2), 214–223.

Hetland, R.D., DiMarco, S.F., 2008. How does the character of oxygen demand control the structure of hypoxia on the Texas–Louisiana continental shelf? J. Mar. Syst. 70, 49–62.

Hetland, R.D., DiMarco, S.F., 2012. Skill assessment of hydrodynamic model of circulation over the Texas–Louisiana continental shelf. Ocean Modell. 43–44, 49–62.

Kara, A.B., Metzger, E.J., Bourassa, M.A., 2007. Ocean currents and wave effects on wind stress drag coefficient over the global ocean. Geophys. Res. Lett. 34, L01604. http://dx.doi.org/10.1029/2006GL027849.

Kirby, J.T., Chen, T.-M., 1989. Surface waves on vertically sheared flows: approximate dispersion relations. J. Geophys. Res. 94, 1013–1027.

Kitaigorodskii, S.A., Donelan, M.A., Lumley, J.L., Terray, E.A., 1983. Wave–turbulence interaction in the upper ocean, part II. Statistical characteristics of wave and turbulent components of the random velocity field in the marine surface layer. J. Phys. Oceanogr. 13, 1988–1999.

Komen, G.J., Hasselmann, S., Hasslemann, K., 1984. On the existence a fully developed wind-sea spectrum. J. Phys. Oceanogr. 14, 1271–1285.

Kudryavtsev, V.N., Grodsky, S.G., Dulov, V.A., Bol'shakov, A.N., 1995. Observations of wind waves in the Gulf Stream frontal zone. J. Geophys. Res. 100 (C10), 20715–20727.

Kumar, N., Voulgaris, G., Warner, J.C., Olabarrieta, M., 2012. Implementation of the vortex force formalism in the coupled ocean–atmosphere–wave–sediment transport (COAWST) modeling system for inner shelf and surf zone application. Ocean Modell. 47, 65–95.

Lentz, S.J., Fewings, M.F., 2012. The wind and wave driven inner shelf circulation. Annu. Rev. Mar. Sci. 4, 317–343.

Longuet-Higgins, M.S., 1970. Longshore currents generated by obliquely incident sea waves: 2. J. Geophys. Res. 75 (33), 6790–6801.

Longuet-Higgins, M.S., Stewart, R.W., 1962. Radiation stress and mass transport in gravity waves, with application to surf beats. J. Fluid Mech. 13, 481–504.

Madsen, O.S., 1994. Spectral wave–current bottom boundary layer flows. In: Coastal Engineering 1994. Proceedings of the 24th International Conference on Coastal Engineering Research Council, Kobe, Japan, pp. 384–395.

Marta-Almeida, M., Hetland, R.D., Zhang, X., 2013. Evaluation of model nesting performance on the Texas–Louisiana continental shelf. J. Geophys. Res. 118, 1–16. http://dx.doi.org/10.1002/jgrc.20163.

Mathisen, P.P., Madsen, O.S., 1996. Waves and currents over a fixed rippled bed: I. Bottom roughness experienced by waves and II. Bottom and apparent roughness experienced by currents. J. Geophys. Res. 101 (C7), 16533–16550.

McWilliams, J., Restrepo, J., Lane, E., 2004. An asymptotic theory for the interaction of waves and currents in coastal waters. J. Fluid Mech. 511, 135–178.

Mellor, G., 2003. The three dimensional current and surface wave equations. J. Phys. Oceanogr. 33, 1978–1989.

Mellor, G., 2008. The depth-dependent current and wave interaction equations: a revision. J. Phys. Oceanogr. 38, 2587–2596.

Morey, S.L., Martin, P.J., O'Brien, J.J., Wallcraft, A.A., Zavala-Hidalgo, J., 2003. Export pathways for river discharged fresh water in the northern Gulf of Mexico. J. Geophys. Res. 108, C10. http://dx.doi.org/10.1029/2002JC001674.

Olabarrieta, M., Warner, J.C., Armstrong, B., Zambon, J.B., He, R., 2012. Ocean–atmosphere dynamics during Hurricane Ida and Nor'Ida: an application of the coupled ocean–atmosphere–wave–sediment transport (COAWST) modeling system. Ocean Modell. 43–44, 112–137.

Orlanski, I., 1976. A simple boundary condition for unbounded hyperbolic flows. J. Comput. Phys. 21, 251–269.

Perrie, W., Tang, C.L., Hu, Y., Detracy, B.M., 2003. The impact of waves on surface currents. J. Phys. Oceanogr. 33, 2126–2140.

Pleskachevsky, A., Kapitza, H., 2009. Interaction of waves, currents and tides, and wave-energy impact on the beach area of Sylt Island. Ocean Dyn. 59, 451–461.
Prandle, D., Hargreaves, J., McManus, J., Campbell, A., Duwe, K., Lane, A., Mahnke, P., Shimwell, S., Wolf, J., 2000. Tide, wave and suspended sediment modeling on an open coast-holderness. Coastal Eng. 41 (1–3), 237–267.
Ris, R.C., Booij, N., Holthuijsen, L.H., 1999. A third generation wave model for coastal regions. 2. Verification. J. Geophys. Res. 104 (C4), 7667–7681.
Salisbury, J.E., Campbell, J.W., Linder, E., Meeker, L.D., Müller-Karger, F.E., Vörösmarty, C.J., 2004. On the seasonal correlation of surface particle fields with wind stress and Mississippi discharge in the northern Gulf of Mexico. Deep Sea Res. II 51, 1187–1203.
Schiller, R.V., Kourafalou, V.H., Hogan, P., Walker, N.D., 2011. The dynamics of the Mississippi River plume: impact of topography, wind and offshore forcing on fate of plume waters. J. Geophys. Res. 116, C06029. http://dx.doi.org/10.1029/2010JC006883.
Sclavo, M., Benetazzo, A., Carniel, S., Bergamasco, A., Falcieri, F.M., Bonaldo, D., 2013. Wave–current interaction effect on sediment dispersal in a shallow semi-enclosed basin. J. Coastal Res. 65, 1587–1592.
Shchepetkin, A.F., McWilliams, J.C., 2005. The regional ocean modeling system: a split-explicit, free-surface, topography-following coordinates ocean model. Ocean Modell. 9, 347–404.
Sheng, P., Liu, T., 2011. Three dimensional simulation of wave-induced circulation: comparison of three radiation stress formulations. J. Geophys. Res. 116, C05021. http://dx.doi.org/10.1029/2010JC006765.
Sheng, Y.P., Zhang, Y., Paramygin, V.A., 2010. Simulation of storm surge, wave, and coastal inundation in the Northeastern Gulf of Mexico region during Hurricane Ivan in 2004. Ocean Modell. 35, 314–331.
Signell, R.P., List, J.H., 1997. Effect of wave-enhanced bottom friction on storm driven circulation in Massachusetts Bay. J. Waterway Port Coastal Ocean Eng. 123 (5), 233–239.
Svendsen, I.A., 1984. Mass flux and undertow in a surf zone. Coastal Eng. 8 (4), 347–365.
Terray, E., Donelan, M.A., Agrawal, Y.C., Drennan, W., Kahma, K., Williams, A.J., Hwang, P.A., Kitaigorodakii, S.A., 1996. Estimates of kinetic energy dissipation under breaking waves. J. Phys. Oceanogr. 26, 792–807.
Uchiyama, Y., McWilliams, J., Shchepetkin, A., 2010. Wave–current interaction in on oceanic circulation model with a vortex-force formalism: application to the surf zone. Ocean Modell. 34, 16–35.
Umlauf, L., Burchard, H., 2003. A generic length-scale equation for geophysical turbulence models. J. Mar. Res. 61 (2), 235–265.
Vincent, C.E., 1979. The interaction of wind-generated sea waves with tidal currents. J. Phys. Oceanogr. 9, 748–755.
Wang, J., Shen, Y., 2010. Development and validation of a three dimensional wave–current coupled model on unstructured meshes. Sci. Chin. Phys. Mech. Astron. 54 (1), 1–17.
Wang, W., Nowlin Jr, W.D., Reid, R.O., 1998. Analyzed surface meteorological fields over the northeastern Gulf of Mexico for 1992–94: mean, seasonal, and monthly patterns. Mon. Weather Rev. 126, 2864–2883.
Warner, J.C., Sherwood, C.R., Arango, H.G., Signell, R.P., 2005. Performance of four turbulence closure models implemented using a generic length scale method. Ocean Modell. 8 (1–2), 81–113.
Warner, J.C., Sherwood, C.R., Signell, R.P., Harris, C.K., Arango, H.G., 2008. Development of a three dimensional, regional, coupled wave current, and sediment transport model. Comput. Geosci. 34 (10), 1284–1306.
Warner, J.C., Armstrong, B., He, R., Zambon, J., 2010. Development of a coupled ocean–atmosphere–wave–sediment transport (COAWST) modeling system. Ocean Modell. 35, 230–244.
Wolf, J., Prandle, D., 1999. Some observations of wave–current interaction. Coastal Eng. 37, 471–485.
Xu, K., Harris, C.K., Hetland, R.D., Kaihatu, J.M., 2011. Dispersal of Mississippi and Atchafalaya sediment on the Texas–Louisiana shelf: model estimates for the year 1993. Cont. Shelf Res. 31, 1558–1575.
Yankovsky, A.E., Chapman, D.C., 1997. A simple theory for the fate of buoyant coastal discharges. J. Phys. Oceanogr. 27, 1386–1401.
Zhang, X., Han, G., Wang, D., Li, W., He, Z., 2011. Effects of surface wave breaking on the surface boundary layer of temperature in the Yellow sea in summer. Ocean Modell. 38, 267–279.
Zhang, X., Hetland, R.D., Marta-Almeida, M., DiMarco, S.F., 2012. A numerical investigation of the Mississippi and Atchafalaya freshwater transport, filling and flushing times on the Texas–Louisiana shelf. J. Geophys. Res. 117, C11009. http://dx.doi.org/10.1029/2012JC008108.
Zhang, W., Hetland, R.D., DiMarco, S.F., Fennel, Katja, submitted for publication. The impact of shelf stratification on hypoxia over Texas–Louisiana shelf. Ocean Modell.
Zhang, Z., Hetland, R.D., Zhang, X., 2014. Wind-modulated buoyancy circulation over the Texas-Louisiana shelf. J. Geophys. Res. 119 (9), 5705–5723.
Zhong, L., Li, M., 2006. Tidal energy fluxes and dissipation in the Chesapeake Bay. Cont. Shelf. Res. 26, 752–770.